Does sporadic permafrost influence catchment-scale groundwater processes?

Laura N. Lyon

Department of Earth and Planetary Sciences

McGill University, Montreal

December 2019

A thesis submitted to McGill University in partial fulfillment of the requirements of the degree of

Master of Science

Table of Contents

List of Figures

List of Tables

Abstract

Groundwater processes in subarctic regions are poorly understood, particularly in areas of sporadic permafrost (perennially frozen ground underlying 0-50% of the landscape). Permafrost acts as an impermeable boundary to groundwater flow and can control porewater movement and storage. The objective of this thesis is to develop a conceptual understanding of how permafrost thaw caused by climate change will impact groundwater flow in watersheds underlain by sporadic permafrost. I use field data from Granger Basin, a headwater catchment in the Wolf Creek Research Basin, Yukon, Canada, to develop an archetypal model using the USGS saturated-unsaturated variable-density groundwater flow model with dynamic freeze-thaw functionality (SUTRA-ice). Capacitive-coupled resistivity and ground penetrating radar were used to map permafrost and depth to bedrock. Simulations show that the presence of permafrost influences patterns of groundwater discharge (exfiltration) to surface water. Specifically, a fill-spill mechanism occurring in late summer where groundwater accumulates upslope sporadic permafrost blocks until it is rapidly released upon reaching a threshold water level. As a result of this mechanism, with the presence of permafrost there is an increase in late summer exfiltration as a result of spill events. As permafrost thaws the fill-spill mechanism is diminished, and within decades there are no longer spill events. The net result is that permafrost thaw can lead to a decrease in late summer groundwater exfiltration, with potential impacts on the subarctic hydrologic cycle including changes in ecohydrology function and water resources.

Résumé

Les mécanismes affectant l'écoulement de l'eau souterraine dans les régions subarctiques sont relativement méconnus, en particulier dans les zones où le pergélisol est sporadique (i.e. 0 à 10% du territoire est couvert par un sol gelé en permanence). Le pergélisol joue le rôle d'une barrière imperméable à l'écoulement de l'eau souterraine et peut par le fait même restreindre le mouvement et l'emmagasinement de l'eau dans les pores du sol. L'objectif de ce projet est de développer une compréhension conceptuelle des impacts de la dégradation du pergélisol sur l'écoulement des eaux souterraines dans les bassins versants subissant des changements climatiques. Des données prises dans le bassin versant Granger, situé dans la partie amont du Wolf Creek Research Basin au Yukon, Canada, ont été utilisés pour développer un modèle avec SUTRA-ice, le code numérique de l'USGS qui simule l'écoulement des eaux souterraines dans les milieux saturés et non-saturés, le transfert de chaleur par conduction, advection et convection et les impacts dynamiques du gel et dégel du sol. Des levés de résistivité électrique et de géoradar ont été réalisés pour localiser le pergélisol et le roc. Les résultats des simulations démontrent que la présence de pergélisol influence les tendances de décharge des eaux souterraines vers la surface (exfiltration). Plus précisément, un mécanisme de remplissage et de déversement (fill-spill) de l'aquifère en amont du pergélisol, où l'eau souterraine s'accumule pour ensuite se déverser rapidement dans l'aquifère en aval lorsque le niveau de la nappe atteint un seuil critique, est observé. Il y a donc une augmentation de l'exfiltration à la fin de l'été, causée par les épisodes de déversement et la présence de pergélisol. L'impact du fill-spill sur l'exfiltration est considérablement diminué alors que le pergélisol se dégrade et, après quelques décennies, il n'y a plus d'épisodes de déversement. Au bout du compte, la dégradation du pergélisol peut mener à une diminution de l'exfiltration des eaux souterraines à la fin de l'été ce qui peut affecter le cycle hydrologique des régions subarctiques et, par le fait même, la biodiversité et les ressources en eaux.

Acknowledgements

This project was funded by the Mountain Water Futures project of the Global Water Futures program. I am grateful to have had the opportunity to work with such an interdisciplinary and dynamic group of professors, graduate students, and technicians who share my passion for hydrology. Huge thanks to my committee member Sean Carey who was always supportive and encouraging, as well as Nadine Shatilla for showing me around Wolf Creek. I would also like to thank the scientists at the Environment Yukon Water Resources Branch Dave Barrett, Tyler de Jong, Katie Pfeifer, and John Miller for supporting my field work.

My thesis would not have been possible without the support and friendship of the 'Laboratory of Advanced Hydrogeological Modeling and Stuff' including Lauren Somers, Rob Wu, Lin Chen, Pan Wu, Leon Koegel, Morgan Sadler, and Audrey Woo. A special thanks to Pierrick Lamontagne-Hallé for sharing his modeling expertise, field skills, and encouraging words; Greg Langston for making my field work possible and staying positive when I thought it wouldn't be; and to Fanny Amyot for sharing her geophysics expertise and always being there when I needed to rant. Thanks to the EPS administrative team Anne Kosowski, Kristy Thornton and Angela Di Ninno for dealing with all my requests keeping everything on track.

It is hard for me to put into words the appreciation I have for my supervisor Jeffrey McKenzie. Without his scientific expertise, positive attitude and good humor my thesis would not have been possible. His unwavering support for my scientific pursuits as well as science adjacent passions allowed me to have a truly enriching graduate school experience. I am blessed to have had such a talented scientist and patient teacher as a mentor and a friend.

And finally, I want to thank everyone from my past and present who has encouraged me to pursue research and taught me how to navigate this crazy world. This includes friends and professors in the Department of Geography, researchers at the STRI, staff at AGU, crew at Restaurant Gus, my amazing friends (especially those who pretended to care about permafrost while sitting through multiple presentation rehearsals), and all of my beloved family members, especially my grandmother Miriam, parents Matt and Chingman, and brother Paul. Special thanks to my patient, endearing, and supportive husband Nick – you're the best teammate one could ask for.

1 Introduction

Arctic and subarctic regions are experiencing hydrologic change as a result of rising temperatures due to climate change. With a trend of increased thawing in the Arctic, groundwater is expected to become more important in the hydrologic regime, though there is very little known about hydrogeologic systems in the north. Due to the impermeable nature of frozen soils and permafrost, groundwater primarily flows above the permafrost table in the seasonally-thawed active layer, or through perennially unfrozen zones called taliks (Walvoord and Kurylyk, 2016). The thawing of permafrost presents a positive feedback loop, where an increase in active layer thickness and talik area allows for more groundwater flow, which in return can induce more thaw (McKenzie and Voss, 2013). Over recent decades, researchers have observed a continuous decrease in the thickness and distribution of permafrost (Osterkamp, 2005; Romanovsky *et al.*, 2010), though the ultimate effects of these changes on groundwater systems are uncertain.

Groundwater is an essential component of northern hydrological systems. It supplies water to rivers, lakes, and wetlands, drives ecohydrological functions and fisheries, and is a key component of water resources. Increases in winter groundwater baseflow and annual discharge are already observed in the north (e.g., St. Jacques and Sauchyn, 2009), but our understanding of groundwater-surface water interactions needs to be improved to predict future responses to climate change. This thesis focuses on utilizing existing data in conjunction with field observations to create a two-dimensional simulation of groundwater flow and heat. The study site, Wolf Creek Research Basin, Yukon Territory, is representative of the interior subarctic cordilleran landscape that has been the focus of many research projects relating to hydrology, biology, and climatology. The basin is underlain by sporadic permafrost, which has unique impacts on northern hydrological processes due to its scattered nature. The research objective is to develop a conceptual understanding of the processes that control groundwater in northern mountain environments with sporadic permafrost, and to assess the long-term impacts of permafrost thaw on hydrologic regimes.

2 Literature Review

2.1 Mountain Groundwater Systems

Almost 40% of the world's population depend on rivers originating in high mountains for their water supply (Viviroli *et al.*, 2019). In high mountain systems, groundwater was arguably neglected in early research and assumed to be a negligible component of the water budget (Somers and McKenzie, *in review*). In the past two decades field-based and modeling studies have shown that mountain groundwater has a critical role in water storage and transport (e.g., Somers and McKenzie, *in review*; Hayashi, 2019). In the hydrologic cycle of the North American Rockies, rivers and streams typically have a short high-flow period during the spring snowmelt (called freshet), followed by a long low-flow period sustained by groundwater discharge. The volume and timing of the snowmelt is highly influenced by the snowpack thickness, spring temperature, and the amount and timing of spring precipitation (Paznekas and Hayashi, 2016). Once headwaters freeze over, groundwater still sustains an almost negligible amount of stream and river flow that is very consistent year to year (often called baseflow). Though freshet is the most significant event for mountain hydrological regimes annually, these low-flow periods are important for aquatic habitats, run-of-river hydropower generation, and downstream water supply (Hayashi, 2019).

Somers and McKenzie (*in review*) identify three main ways that groundwater processes in mountain regions differ from lower elevation sites. First, flow paths and discharge rates are influenced by higher hydraulic gradients (Forster and Smith, 1988). Second, due to the high-energy depositional environments and glacial processes in mountain regions, the near surface hydrogeologic stratigraphy can be more complex (Cairns, 2014). Finally, the higher relief of surface topography allows for deeper groundwater systems, recharging both local systems and regional and continental scale flow systems, with potential influence from the geothermal temperature gradient (Forster and Smith, 1988).

Within mountain environments, mountain or alpine permafrost can form. Permafrost is frozen ground where temperatures are perennially below 0 °C. It is typically found in northern latitudes (typically over 60°N) and high elevations. In high latitudes, permafrost is sporadic and exists due to low temperatures and minimal snow cover (Zhang, 2005). It has been proposed that regardless of latitude, mountains over 500 m in elevation such as the Rocky Mountains, Alps, Pamirs, Tien

Shan, Altai, and the mountain regions of Mongolia and Japan, can also contain discontinuous or sporadic permafrost (Gorbunov, 1978). Its existence in high altitudes is closely linked to climate (Guodong and Dramis, 1992) and one third of global permafrost is found in mountainous terrain (Hock et al., *in press*).

2.2 Permafrost Hydrology

Currently, approximately 24% of terrestrial land in the Northern Hemisphere is underlain by permafrost (Lemke *et al.*, 2007), but this number is decreasing rapidly as climate warming induces thaw. There are four classifications for permafrost distribution based on the area as a percentage of the total landscape: continuous (90-100%), discontinuous (50-90%), sporadic (10-50%), and isolated (0-10%) (Brown *et al.*, 1998). Though the boundaries between the different permafrost classification zones can be ambiguous, subarctic regions generally contain sporadic or discontinuous permafrost. This thesis will be focused on sporadic permafrost.

2.2.1 Sporadic Permafrost

Sporadic permafrost is found in high latitudes and elevations, generally due to cold temperatures and thin snow cover (potentially as the result of blowing wind). Snow is a strong insulator and can significantly insulate soil temperatures. On the North Slope of Alaska, Zhang *et al.* (1997) found that fresh, low density snow could keep the mean ground surface temperature 20 °C warmer than the mean monthly air temperature. Snow can insulate over six times more effectively than soil for equivalent depths due to its extremely low thermal conductivity, making the depth and density of the snowpack very important for permafrost distribution (Pomeroy and Brun, 2001). In the western mountain ranges of North America, low winter snow cover and high winds are major factors for promoting permafrost formation (Harris and Giardino, 1993). The timing of snowfall events in relation to the winter drop in air temperatures is significant for the ground thermal regime (Zhang, 2005). Thick snowpack formation prior to extensive heat loss in the ground can create unfavorable conditions for permafrost development. Mountain environments that consistently have heavy winter snowfall will typically develop glaciers rather than permafrost where cool ground surface temperatures are required (Harris and Corte, 1992). In high latitudes, peatlands can also drive sporadic permafrost formation due to insulation from dried peat in the summer, and heat loss driven by the high thermal conductivity of ice-rich peat in the winter (Zhang, 2005). The patchy development of sporadic permafrost creates a heterogeneous landscape with scattered impermeable boundaries for groundwater flow.

2.2.2 The Impact of Slope Aspect in Subarctic Environments

In high latitudes, north and south facing slopes exhibit different hydrologic processes as a result of south facing slopes receiving more solar radiation. The slope aspect drives variation due to vegetation, soil surface cover (organic mat vs. leaf litter), frozen ground conditions, snowpack thickness, snowmelt timing, and runoff mechanisms (Carey and Woo, 1998). Permafrost generally does not form beneath south facing slopes or flat pasture due to dry soil moisture conditions and warmer summer soil temperatures (Ishikawa *et al.*, 2005).

A study of two hillslopes in the subarctic Wolf Creek Research Basin, Yukon Territory, Canada by Carey and Woo (1998) examined the differences between a north and south facing slope. Results showed that the north facing slope, which was underlain with permafrost, exhibited shallow subsurface flow confined to the active layer during freshet. Due to the thin organic layer of the slope, water can infiltrate the frozen organic soil, but the ice rich substrate blocks deep percolation. Runoff processes on the north facing slope are lateral, travelling along intermittent rills fed by diffuse and pipe flows. For the south facing slope, snow meltwater can infiltrate the frozen silt without generating runoff due to it only being underlain by seasonal frost. Evans and Ge (2017) showed that hillslopes with seasonally frozen ground typically have more discharge due to the larger temporal window of potential infiltration, but with climate warming permafrost slopes will experience the highest percentage of change in discharge due to increasing active layer thickness.

2.3 Groundwater in Permafrost Environments

Hydrogeologically, frozen ground, including permafrost, acts as an impermeable boundary to groundwater flow due to ice-filled pores blocking groundwater flow (Williams and Smith, 1989). When pore ice melts, it increases permeability which can change groundwater flow rates and patterns and increase the infiltration rate of surface water into the ground. Permafrost limits shallow groundwater flow to the seasonally thawed active layer above it and taliks. Deeper groundwater systems exist below the permafrost layers, known as sub-permafrost aquifers (Woo, 2012). Combinations of these flow systems can sustain perennial flow networks between aquifers and surface waters through unfrozen pathways (Walvoord and Kurylyk, 2016).

2.4 Permafrost Thaw and Impacts

Rising temperatures at northern latitudes are already triggering permafrost warming and thawing, with models showing potential large-scale losses of near-surface permafrost (Slater and Lawrence, 2013). Climate models predict that 29-90% of the area that is currently underlain by permafrost will lose a significant amount in the next 80 years, with most areas becoming permafrost-free by 2300 (McGuire *et al.*, 2018). As this happens, permafrost hydrogeology will be transformed in some regions, changing the role of groundwater in northern basins. Two major changes that could occur are (1) newly formed open taliks will facilitate flow between sub and supra-permafrost aquifers, draining lakes and wetlands and (2) increased recharge and discharge through newly activated aquifers can lead to expanding surface water bodies (Walvoord and Kurylyk, 2016). Increased groundwater flow due to the thickening of the active layer can also create a positive feedback due to heat advection, further accelerating the rate of permafrost thaw (McKenzie and Voss, 2013). There is still much uncertainty on how northern watersheds will respond because of nonuniform permafrost degradation and the heterogeneity of northern landscapes.

Studies have reported increases in mean annual discharge and baseflow from northern rivers, showing increased connectivity occurring as permafrost thaws (Walvoord and Striegl, 2007; Déry *et al.*, 2009; Connon *et al.*, 2014). Bense *et al.* (2009) used a numerical model to examine increases in Arctic river discharge, noting that the increase can be attributed to shallow supra-permafrost groundwater systems, but as permafrost thaws deeper flow paths can also form. Muskett and Romanovsky (2009) showed using remote sensing that in Arctic basins when there is permafrost and talik development, 80% of river discharge is baseflow. But when there is a higher percentage of permafrost and poorly developed talks underlying the basin, only 50-60% of total discharge is baseflow in the early summer. Later in year the proportion increases to similar values as low-permafrost basins later due to differences in storage. The literature highlights that new pathways and increases in storage due to permafrost thaw will continue to influence northern hydrology. Ge *et al.*, 2011 showed that there could be increases in groundwater flow due to increased warming, but only if there is enough upgradient water to replenish shallow groundwater systems. Studies show that overall there will be increases in precipitation, notably an increase in rainfall and decrease in snow, which will affect the timing and storage of major recharge events (Callaghan *et al.*, 2011; Bintanja and Andry, 2017), Wetland systems are expected to experience shifts in distribution as well. For example, Lamontagne-Hallé *et al.* (2018) showed through models that the thickening of the active layer can affect wetland distribution due to changes in discharge along the slope.

Permafrost thaw will impact northern communities, physically changing the landscape and potentially water sources. Slope instability and land subsidence will impact infrastructure (Kurylyk, 2019). While new groundwater pathways and taliks may impact water sources by draining lakes and wetlands (Smith, 2005), they may also enhance groundwater availability in other areas and open new water resources for northern communities (Lemieux *et al.*, 2016).

2.5 Hydrogeological Modelling

Similar to mountain watersheds, subarctic and Arctic environments are challenging to study, monitor, model, and extract data from due to extreme conditions and often very remote access. The result is a general shortage of northern groundwater data, and for sites where data does exist, there is typically a short time series preventing in depth analyses (Woo *et al.*, 2008). One tool to overcome these limitations is using numerical groundwater models designed for cold regions, often called cryohydrogeologic models. These models have become an important tool to study how these environments function and will change over time. Cryohydrogeologic models are typically coupled models that simulate groundwater flow and energy transport simultaneously and includes dynamic freeze-thaw effects (Grenier *et al.*, 2018). Groundwater flow mechanisms are typically based on a multidimensional form of Darcy's equation, while the energy transport equation is used to describe heat transfer through conduction, advection, and latent heat released or absorbed through freezing and thawing (Lamontagne-Hallé *et al.*, *in review*). Often these models are archetypal with an aim to develop a conceptual understanding of cold-regions groundwater systems and how they will respond to warming (Bense *et al.*, 2012; Frampton *et al.*, 2013; McKenzie and Voss, 2013; Lamontagne-Hallé *et al.*, 2018). Due to the challenges associated with cryohydrogeological research, there is very little field validation and application of these models.

3 Site Description

The Wolf Creek Research Basin is approximately 15 km southwest of Whitehorse, Yukon (60°30′N, 135°10′W) and is a part of the Yukon River Watershed (Carey and Woo, 1998; **Error! Not a valid bookmark self-reference.**). The basin drains an area of 200 km^2. Average annual temperature is -3 °C and it receives around 350 mm of precipitation annually, with about 40% falling as rain (Sicart *et al.*, 2006). Established as a field research site in 1992, over 25 years of discharge data exist for this watershed, along with results from vegetation, snow survey, and water chemistry studies. Since most studies have focused on surface processes, the nature of regional hydrogeology is not well understood.

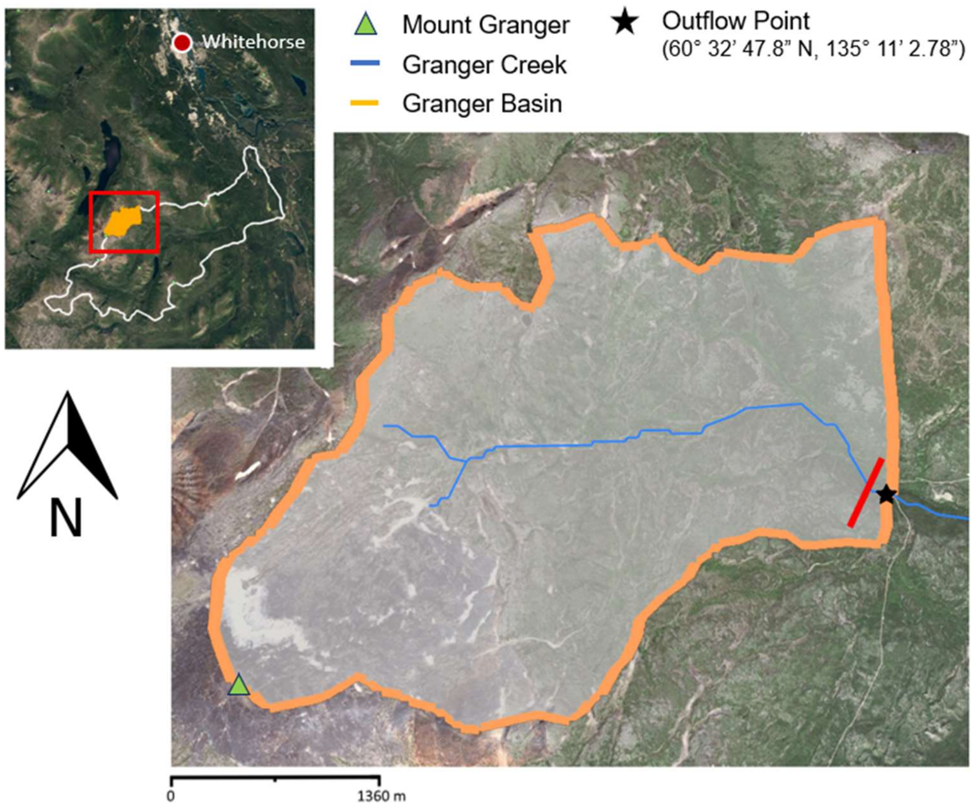

Figure 1. Map of Granger Basin with insert showing location within the Wolf Creek Research Basin relative to Whitehorse, Yukon Territory, Canada. Red line marks the transect used for field data collection. Imagery source: Google Earth

This research project focuses on Granger Basin, a headwater catchment with an area of approximately 7.6 km^2 (60°31′ N, 135°11′ W) and an elevation range of 1,310 to 2,250 m above sea level (Carey *et al.*, 2013). The geology of the basin is primarily sedimentary, consisting of limestone, sandstone, and conglomerate overlain by glacial till. In the central part of the Wolf Creek Research Basin where Granger Basin is located, greywacke, arkose, quartzite, conglomerate, siltstone, argilite, hornfels of the Laberge Group of Lower Jurassic and later ages outcrop along with glacial deposits and wind-blown material (Seguin *et al.*, 1998). Previous studies have predicted that 50-90% of the basin is underlain with permafrost (Lewkowicz and Ednie, 2004). Granger Basin has been the subject of multiple hydrological studies since the inception of Wolf Creek research (Carey and Quinton, 2004; McCartney *et al.*, 2006; Dornes *et al.*, 2008; Shirazi *et al.*, 2009; Boucher and Carey, 2010; Carey *et al.*, 2013; Lessels *et al.*, 2015). The basin contains both north and south facing slopes, which affect permafrost distribution patterns due to the basin's northern latitude. Carey and Woo (1998) showed that slope aspect can determine what hydrologic processes dominate northern hillslopes due to the different amounts of solar radiation that reaches the surface. The warmer south-facing slopes typically only have seasonal frost and are dominated by vertical flow processes while north-facing slopes are dominated by lateral flow processes due to sporadic or discontinuous permafrost.

Though Granger Basin is relatively well studied, groundwater research has been primarily on the near-surface unsaturated zone composed of organic material, where shallow groundwater flow occurs on the north-facing slope, and infiltrates deeper into the mineral soil on the south-facing slope (Carey and Woo, 1998). This thesis will focus on the deep groundwater system (below 1 m) that is saturated year-round and how this system is integrated into the larger hydrological system in subarctic environments.

4 Methods

4.1 Geophysical Data Collection

To develop an understanding of subsurface permafrost distribution and depth to bedrock to serve as a foundation for our cross-sectional numerical model, geophysical methods were used to image the subsurface. A combination of capacitive coupled resistivity (CCR) and ground penetrating radar (GPR) surveys were used to identify permafrost and bedrock features, similar to the methodology used in De Pascale *et al.* (2008) and Angelopoulos *et al.* (2013). The primary survey line was along a transect perpendicular to Granger Creek near the mouth of the basin. Upon processing the data, a final product was created by combining the results of the two datasets. Attempts to validate the geophysical results using a portable auger failed due to terrain difficulties (Supplementary Materials 1).

4.1.1 Data Acquisition

Capacitively Coupled Resistivity (CCR) surveys were made on March 26 and 27, 2018. Three survey lines were captured: the first two-thirds up the north-facing slope of the basin to the western bank of Granger Creek, the second continuing along the same line from the eastern bank of Granger Creek to two-thirds up the south-facing slope, and the third east-west line parallel to Granger Creek on the west bank (Figure 2). The first two lines were combined to produce a north-south transect totaling 500 m, while the east-west line was 370 m. To collect the data, I used the OHM Mapper resistivity mapping system by Geometrics Ltd. Using a dipole-dipole configuration, I surveyed each line with one transmitter and five receivers spaced at 10 m intervals.

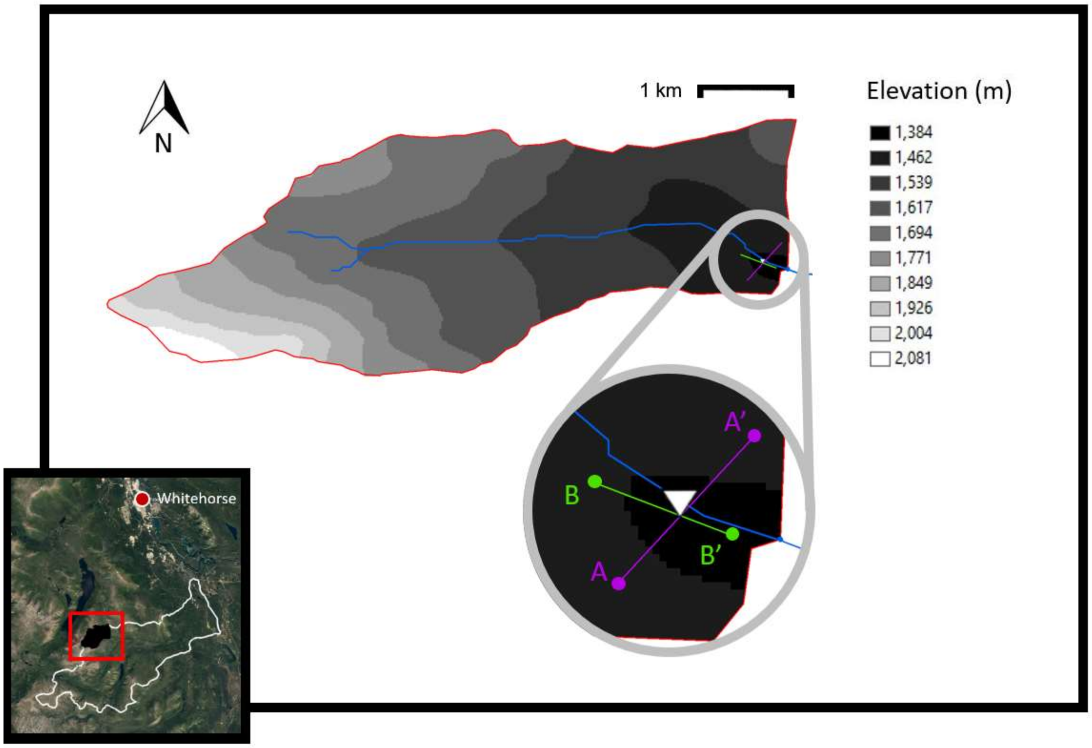

Figure 2. Map of geophysical survey transects within Granger Basin. A-A' is a north-south transect and B-B' is an east-west transect.

GPR surveys on July 5 – 8, 2018, captured lines totaling 570 m following the north-facing and south-facing slope transects used for the CCR surveys. No GPR data was collected along the east-west transect along the stream. The Sensors & Software pulseEKKO GPR system with a 50 MHz rough terrain concept antenna was used to survey 8 GPR lines with a transmitter and receiver spacing of 2 m. Survey points were later taken with a Topcon Differential Global Positioning System (DGPS) in Real-Time Kinematics (RTK) with two GRS5+ GPS antennas and corrected with the Magnet Field software.

4.1.2 Data Processing

For the resistivity data, pseudosections were generated in MagMap2000 and then imported into the inversion software RES2DINV to produce two-dimensional resistivity models (Loke and Barker, 1996). Data was inverted using the robust inversion method which is well suited for areas with sharp stratigraphic boundaries like areas of frozen and unfrozen soil (Langston *et al.*, 2011).

The inversion cell width was set to 5 m, with half electrode spacing and a damping factor of 0.3. The raw data from the north and south facing slopes were combined and inverted together creating one cross-section, while the east-west line was inverted separately.

GPR data was processed after correcting for topography using adapted methodology from Neal (2004) in Ekko View Deluxe (Sensors & Software, 2003) and Ekko Project (Sensors & Software, 2011). To remove unwanted low-frequency data a DeWow filter was applied. Data was then migrated to 0.11 m/ns, chosen from tabular data as a compromise between dry sand, silt, gravel, and permafrost (Neal, 2004; Annan, 2005; Reynolds, 2011). A hyperbola fitting analysis confirmed this value where multiple hyperbolas were fitted for a mean of 0.1087 m/ns. Finally, a bandpass filter was applied to limit frequencies used in the cross-section to a maximum of 100 MHz.

4.2 Model Development and Configuration

4.2.1 Freeze-Thaw Simulation Details

The numerical groundwater modeling for the Granger Basin utilized the SUTRA-ice version of the USGS Saturated-Unsaturated Transport Model (SUTRA) (Voss and Provost, 2002). The code is a finite element numerical model that simulates groundwater flow and heat transfer and is modified to incorporate the hydrologic effects of dynamic freezing and thawing (McKenzie et al., 2007). The code has been used in multiple cryohydrogeologic heuristic studies (e.g., McKenzie and Voss, 2013; Briggs *et al.*, 2014; Kurylyk *et al.*, 2016; Evans and Ge, 2017; Lamontagne-Hallé *et al.*, 2018) and also for simulating research field data (Ge *et al.*, 2011; Zipper *et al.*, 2018). See Supplementary Material 2 for more information.

4.2.2 Model domain, mesh, and boundary conditions

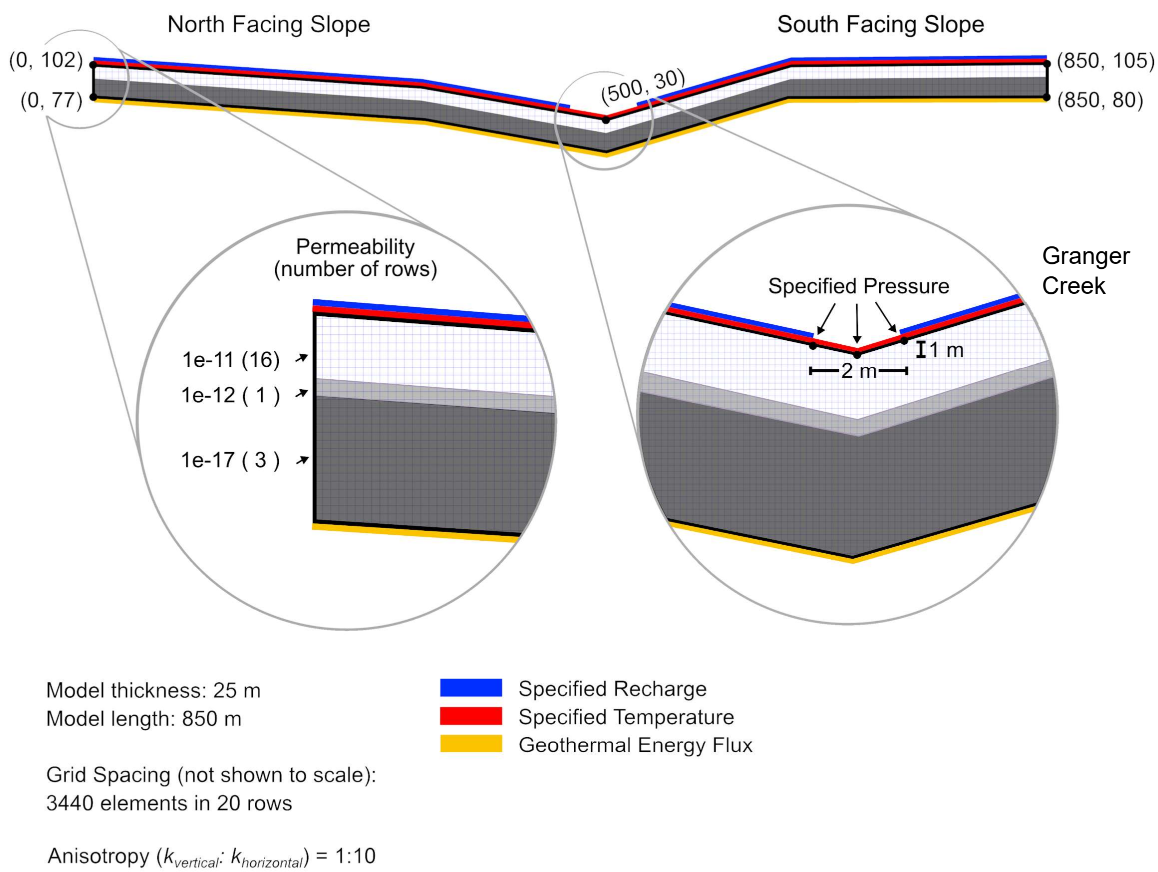

Figure 3. Model domain (no vertical exaggeration) with finite-element mesh and boundary conditions. Shades of grey correlate with layer permeability. Model parameters given in Table 1.

The model represents a two-dimensional cross-section, following the North-South geophysics transect across Granger Basin. The model domain is 850 m long, extending from the southern edge of the basin watershed boundary to the northern edge, with varying topography based on measured values using a Differential Global Positioning System (DGPS; Figure 3). The cross-section has two distinct slopes representing the north and south-facing slopes, divided by Ganger Creek near the center. The model is consistently 25 m thick across the entire domain, with three bands of vertical model grid spacing.

Table 1. Parameters used in freeze/thaw simulations

Parameter	Value
Ice	
Ice specific heat (J/kg)	2,108
Ice thermal conductivity [(J/(s m °C)]	2.14
Density of ice (kg/m^3)	920
Latent heat of fusion (J/kg)	334,000
Liquid water	
Fluid specific heat (J/kg)	4,182
Fluid thermal conductivity [(J/(s m °C)]	0.6
Fluid compressibility [(kg/(ms^2)]$^{-1}$	4.47x10^{-10}
Solid matrix	
Solid grain specific heat (J/kg)	840
Solid grain thermal conductivity [(J/(s m °C)]	3.5
Solid grain matrix compressibility	1x10^{-8}
Density of solid grains (kg/m^3)	2,600
Porosity (-)	0.1
Other	
Gravity (m/s^2)	-9.81
Longitudinal dispersivity	0.5
Transverse dispersivity	0.5
Freezing function	
Type	Exponential
Minimum liquid saturation (-)	0.05
Temperature at which minimum liquid saturation occurs (°C)	-2
Permeability of frozen regions, irrespective of ice saturation (m^2)	10^{-40}
Bottom boundary geothermal energy flux	
Energy source [(J/s)/m^2]	0.085

The model spatial discretization is 0.5 m deep x 5.0 m wide finite elements for the top band of elements, 2.0 m x 5.0 m in the middle band, and 5.0 m x 5.0 m in the bottom band. The top two bands of elements represent a 10 m thick layer of overburden, while the bottom band represents a 15 m thick bedrock layer. The depth to bedrock is based on the results of the geophysical surveys and is assumed to be constant. Permeability corresponds to the element band, with the top having a permeability of 1 x 10^{-11} m^2, middle band 1 x 10^{-12} m^2, and bottom band of 1 x 10^{-18} m^2 with all bands having 1:10 anisotropy. Hydrogeologic parameters correspond to field data collected near the field site and literature values of similar materials (**Error! Reference source not found.**;

Yukon Observational Well Network, 2001). Additional simulations used to assess conduction-only thaw processes had all permeabilities set to 1 x 10^{-40} m^2.

The vertical boundaries at the outer edges of the model correspond to the watershed boundaries of Granger Basin and are assumed to have no water flow and no heat flux. The bottom boundary of the domain has a no-flow condition and a specified heat flux of 0.085 W/m^2 representing the geothermal heat gradient (McKenzie and Voss, 2013).

The surface-layer boundary is divided into three sections, the north-facing slope, Granger Creek, and the south-facing slope (Figure 3). For the north and south facing slopes, the land surface is represented by a combination of hydraulic drain, specified temperature flux, and specified recharge boundary conditions. Specified temperature flux and recharge inputs are based on field data from two meteorological stations on the north and south facing slopes of Granger Basin from 1998-2002 (Wolf Creek Hydrometerological Database, 2011a, 2011b). For each of the slopes, daily average data from 5 cm soil depth was used directly as the specified temperature to incorporate the effects of the surface energy balance due to snow insulation, albedo, and vegetation on ground temperature not being simulated by the current version of SUTRA-ice. Daily average parameters were calculated from the field datasets, which had measurements with a 30-minute period. Small data gaps were filled using linear interpolation and gaps during significant seasonal changes (i.e. freshet) were filled in using another year with similar temperature patterns (Figure 4). The model used hydraulic drain nodes, implemented as described in Lamontagne-Hallé *et al.* (2018), in order to remove water when pressures in the top row of nodes exceeds 0 Pa.

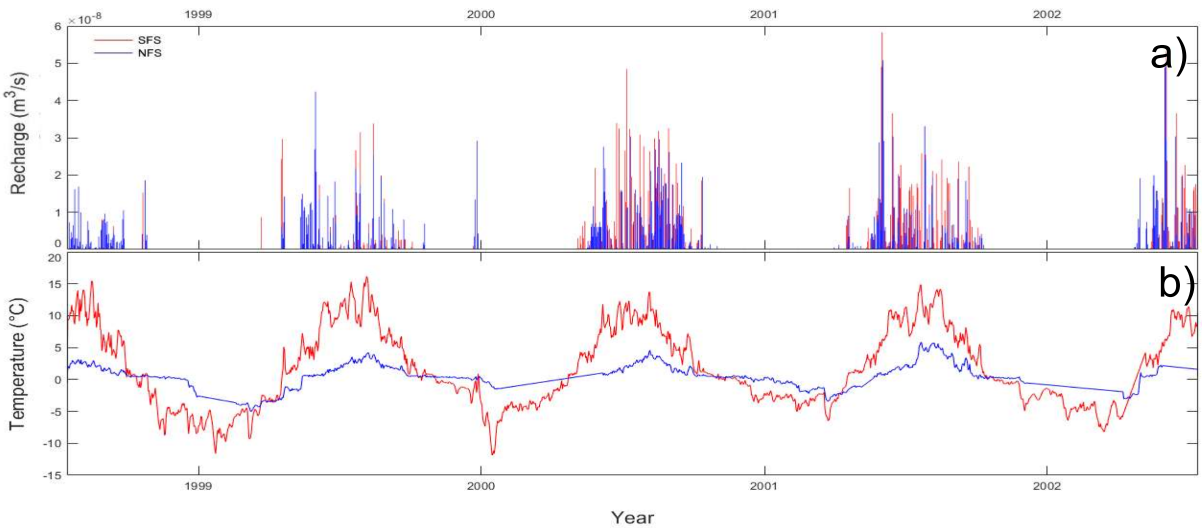

Figure 4. Recharge (a) and 5 cm soil temperature (b) from the north (blue) and south (red) facing slopes of Granger Basin from July 1998 to July 2002.

Daily recharge data for the model is based on 30-minute snow depth and rainfall datasets from Granger Creek. For snowmelt, a daily melt value is determined by the difference in snow depth between two days at 12:00 AM. Snowmelt recharge is calculated by converting snow-water equivalent (SWE) assuming a snow bulk density of 0.25 kg/m^3, an average value for Granger Basin (Carey and Woo, 2001). For rainfall, the daily value used for the simulations is the sum of the rainfall values over the entire day. I assume that only 20% of rainfall and 10% of snowmelt becomes groundwater recharge due to sublimation, evapotranspiration, interception from vegetation, and surface runoff during freshet (Clilverd *et al.*, 2011).

Previous studies on snow mass balance at Wolf Creek show that 17-46% of snowfall can be lost to blowing snow transport and sublimation (Pomeroy *et al.*, 1998). South-facing slopes typically have little spring runoff due to high evaporation, while the north-facing slopes have a thin frozen organic layer that impounds infiltration and induces surface runoff in rills and gullies and subsurface runoff within macropores of the organic soil (Carey and Woo, 1998). Daily groundwater recharge comes from rainfall or snowmelt depending on the time of year. When snow depth is increasing and rainfall data is recorded, I assume it is snow and no daily recharge value is input to the model. When snow depth is decreasing and there is rainfall, I assume there is a rain on snow event and recharge comes from both snowmelt and rainfall.

Table 2. Average, high, and low temperature and proportion of rain and snow recharge values for each climate input scenario (S1-S5) constructed from Granger Basin field data.

	North Facing Slope							South Facing Slope						
	Temperature (°C)			Recharge (mm/year)		Recharge Source		Temperature (°C)			Recharge (mm/year)		Recharge Source	
	Average	High	Low	Rain	SWE	Rain	Snow	Average	High	Low	Rain	SWE	Rain	Snow
S1 (1998-99)	-0.51	3.12	-5.02	20.76	30.52	40%	60%	0.78	15.47	-11.62	20.14	5.36	79%	21%
S2 (1999-00)	0.64	4.25	-1.54	35.34	18.24	74%	38%	1.88	16.15	-11.82	44.80	28.90	61%	39%
S3 (2000-01)	0.36	4.59	-3.45	64.32	22.24	74%	26%	2.01	13.75	-6.46	63.34	29.30	68%	32%
S4 (2001-02)	0.53	5.85	-3.03	46.96	17.49	73%	27%	1.75	14.90	-8.20	45.58	36.28	56%	44%
S5 (1998-02)	0.26	5.85	-5.02	41.84	22.12	65%	38%	1.60	16.15	-11.82	43.47	24.96	66%	34%

After combining the daily input datasets for 5 cm soil temperature, rainfall, and snowmelt, I identified four annual climatic regimes (S1 through S4) for individual years (July 15^{th} to July 14^{th} of the subsequent year), that each have continuous usable data with a separate input for the north and south slope (Table 2): S1 (1998-1999) was a relatively cold dry year, S2 (1999-2000) had average temperatures but very little recharge, S3 (2000-2001) was an average wet year, and S4 (2001-2002) was a warm year with average recharge. A fifth scenario, S5, consists of the four years (S1 through S4) repeating in sequence (1998-2002).

For each model run, I use one of the five S scenarios, with the specified surface temperature flux and specified recharge, repeating for 100 years. The approach of repeating one year of data was made because of the limited continuous data that exists for both the north and south facing slopes simultaneously. To observe the system in a more natural state, S5 was created, which combines years that ranged in recharge and temperature. This allows comparison of the static S1-S4 runs to the more dynamic S5 run and observe how the behavior of the antecedent years impacts groundwater discharge patterns of the next year. See Figure 5 for an outline of how field data was incorporated into the modeling process.

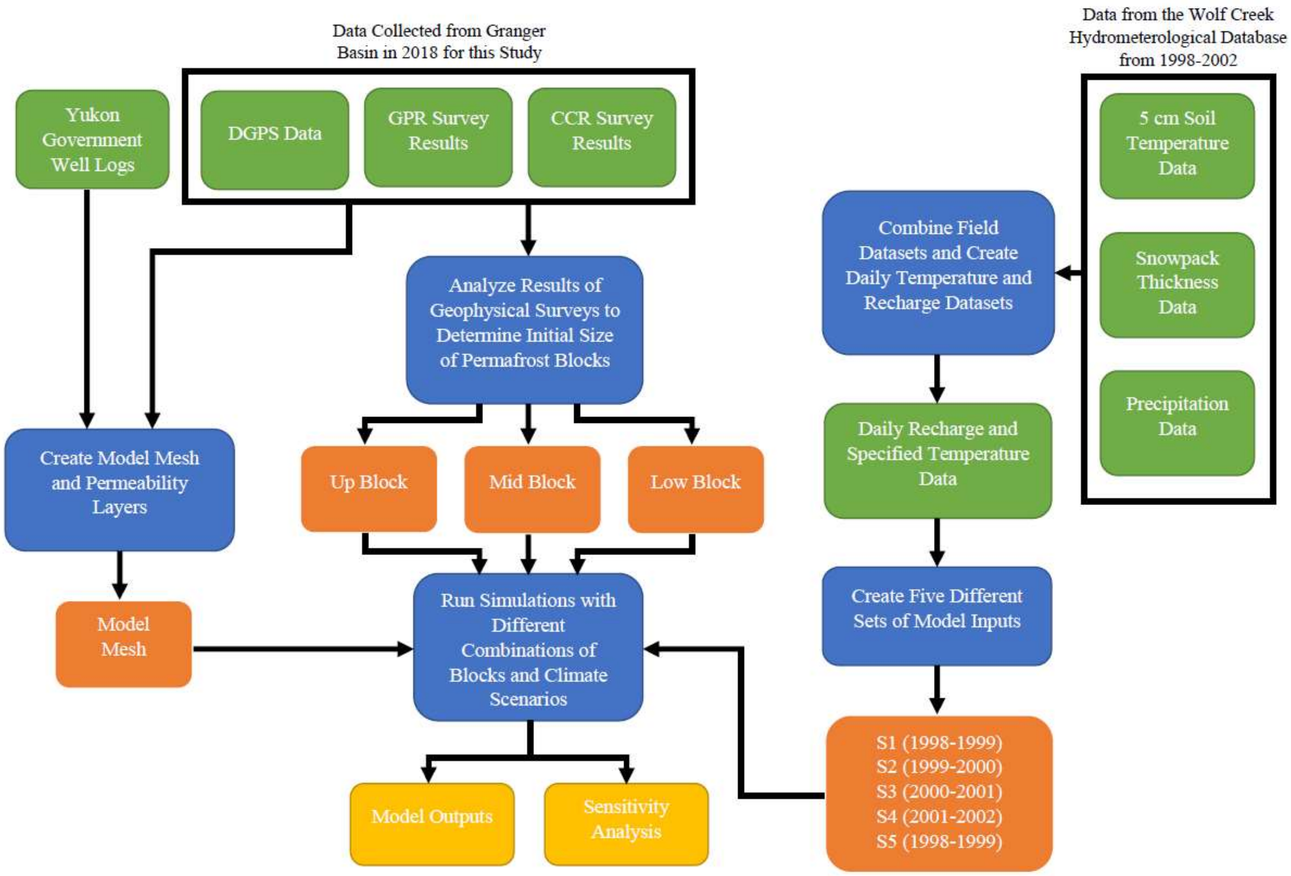

Figure 5. Flowchart of model development. Field data (green blocks) was used to develop the model mesh as well as model inputs (orange blocks). Yellow blocks represent model results, while blue blocks represent methods for data processing and modeling.

Granger Creek is represented by a 2 m wide by 1 m deep specified pressure (0 Pa) boundary set near the middle of the cross-section at the lowest elevation on the top (land surface) of the model, across three nodes (Figure 3). With the right node held at 0 Pa to represent the top of the water column, the left and center nodes are held at hydrostatic pressure.

4.2.3 Sporadic Permafrost Distribution

Results from the geophysical surveys were used to derive the initial permafrost distribution used in the simulations. The survey results show a block of sporadic permafrost approximately 40 m wide and 7 m thick, which was as part of the initial thermal conditions of the model. For the model I assumed the permafrost block ends at the point of contact between the overburden and bedrock since deeper permafrost would not have an impact on the flow system, and later validate this through sensitivity analyses.

To understand and quantify the impact of the sporadic permafrost, I experimented with running the simulations with different permafrost distributions. I undertook a sensitivity analysis using different combinations and locations of one to three sporadic permafrost blocks. With the original permafrost block from the field results as a size reference, I created three alternate permafrost configurations; the ‘upper block’ which starts 60 m from the left boundary of the model, the ‘middle block’ that starts 180 m from the left boundary, and the ‘lower block’ which starts 255 m from the leftmost boundary (Figure 6). The locations of these permafrost blocks were determined by running simulations with the different temperature scenarios on fully frozen cross-sections and observing which locations were last to thaw. Under all five specified temperature and recharge scenarios, a total of eight simulations were run; three with a single permafrost block, three with the different combinations of the two blocks, one with all three blocks, and one with none. The permafrost blocks were created during the spin-up phase of model simulation.

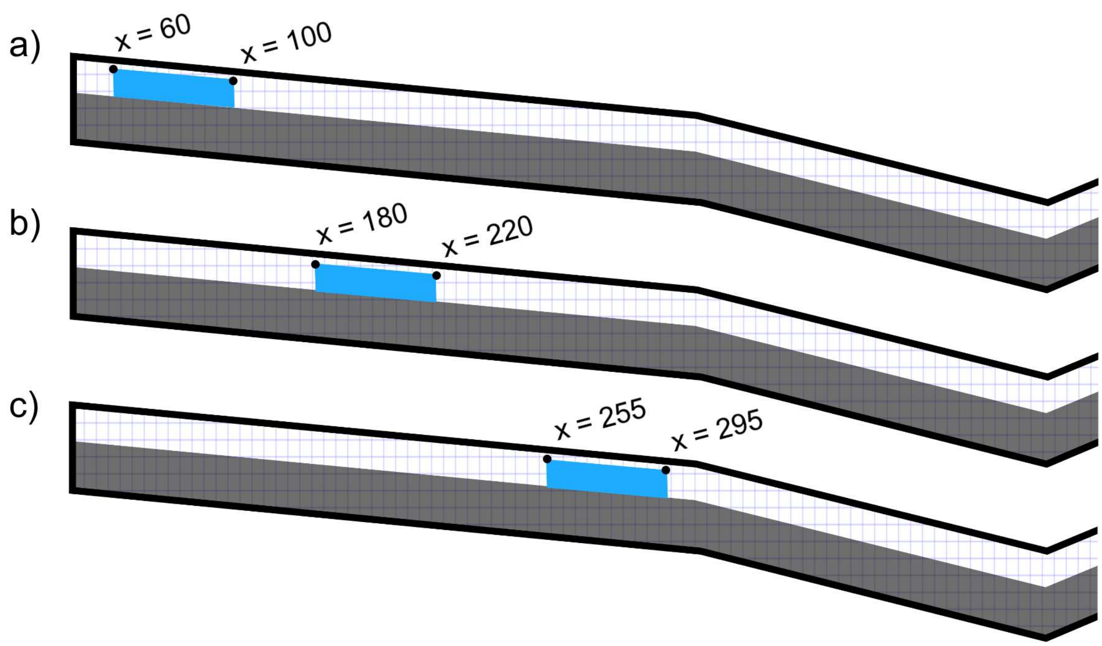

Figure 6. Sporadic permafrost block configurations used in modeling experiment; (a) upslope block, (b) middle block, (c) lower permafrost block. NOTE diagram is not to scale, x = 0 at the left edge of the diagram.

4.2.4 Modeling Sequence

Simulations were run in three steps, the first two steps being sequential spin-up runs to generate the initial conditions, and the third step to produce the model results that are then analyzed. The first step generates the starting pressure distribution across the model and freezes the entire domain. First, specified pressure nodes of 0 Pa and temperature specified temperature nodes of 1 °C were both used at the land surface to generate hydrostatic pressure across the domain. The model was run with saturated conditions for 400,000 years with 50-year time steps. Next, the specified temperature boundary was changed to -2 °C and the geothermal heat gradient applied to the bottom of the domain, and the model is run with saturated-unsaturated conditions for an additional 400,000 years with 50-year time steps.

For step two, specified temperature nodes of -1 °C were applied to the subsurface nodes corresponding to the locations of the previously mentioned sporadic permafrost blocks to create the individual blocks. These runs included specified temperature, specified recharge, and drain nodes at the land surface. Using the input data from Granger Basin from S3 (2000-2001) the three zones (north-facing, south-facing, and creek) were added. Data from S3 was used because it was the most complete dataset and the north facing slope temperature regime for this year was effectively the average relative to the four years of data (Figure 4). Phase two was run for 200 years at 2-hour timesteps, with the same year of data as input for the model. Based on testing, 200 years is required for the model to reach dynamic equilibrium.

Step three consisted of simulations that produced the results, using the five field input datasets for recharge and temperature flux. For S2-S4, the model is run for 100 years at 2-hour timesteps with the same year of data repeating allowing for the complete thawing of the sporadic permafrost blocks. For S5 the model is run for 100 years at 2-hour timesteps with years S1-S4 repeating, and S1 was run for 200 years at 2-hour timesteps due to the lower temperatures specific to that year.

4.2.5 Sensitivity Analysis

A ‘one-at-a-time’ sensitivity analyses of model permeability and sporadic permafrost block thickness is used to demonstrate that simulated groundwater discharge patterns are not specific to the model configuration. For permeability, 13 runs with different permeability magnitudes and differences between the overburden and bedrock layer permeabilities were tested. The depth of the sporadic permafrost block was tested with five different runs, with the sporadic permafrost block extend deep into the bedrock or not touch the bedrock to varying degrees. For each simulation, only one parameter is altered while all others remain constant.

5 Results and Analysis

5.1 Results of Geophysical Surveys

The CCR results show different resistivities for the north and south facing slopes and show a contact layer that could be used to infer the depth to bedrock. The results also include a highly resistive unit that could be permafrost (
Figure 7). For the analysis, I used resistivity values from
Hauck and Kneisel (2008); groundwater has a resistivity of 10-300 Ωm while frozen sediment, ground ice, and mountain permafrost can range from 1 x 10^3-10^6 Ωm. The lines generally reached a depth of 30 m, but a depth of investigation analysis was not performed.

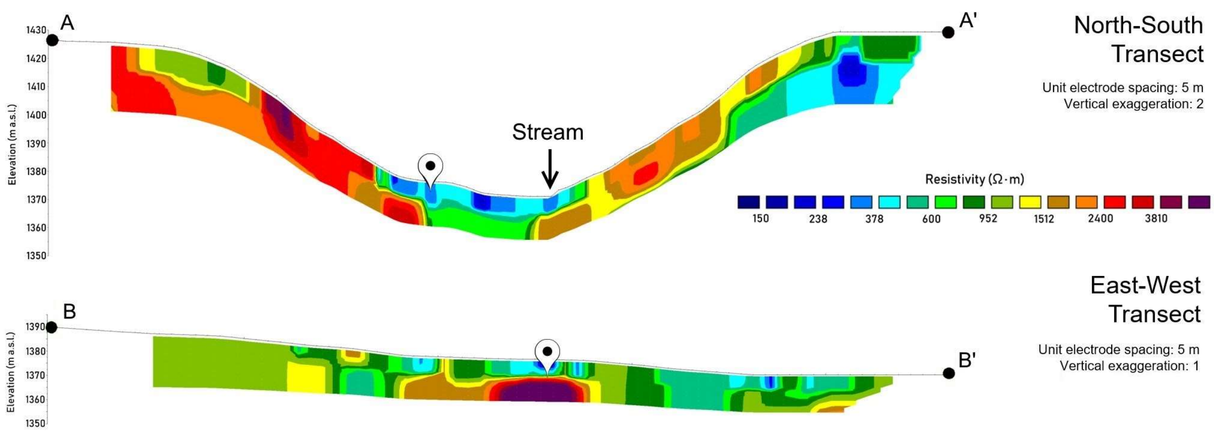

Figure 7. Resistivity of the north-south (A-A') and east-west (B-B') transects. The white location pin indicates where the two transects intersect. For A-A', A at the southernmost end of the transect (i.e. at the top of the north facing slope) and A' is on the northernmost end of the transect (i.e. at the top of the south facing slope). B is the western terminus of the east-west line and B' is the eastern end. The location of the stream is labeled on transect A. For information on the location of the transects, see Figure 2.

For the east-west transect, resistivity values generally range from 370-950 Ωm, except for a highly resistive (>3810 Ωm) unit at the point where the two transects intersect and small pockets of low resistivity (<370 Ωm) near the ground surface. The lower resistivities could be due to the line's proximity to the stream, which is visible in the north-south transect as well. Approximately 10 m below the ground surface, there is a strong resistivity contrast that could represent the depth to bedrock.

For the north-south transect, the south facing slope had resistivity values ranging 600-2400 Ωm, with a significantly less resistive section at the top of the slope (<230 Ωm) that could potentially be a perched aquifer since the resistivity values correspond to those of groundwater. The north facing slope is more resistive, with values over 2400 Ωm. These values are interpreted to indicate that the north facing slope has more frozen sediment and permafrost than the south facing slope, which corresponds with results from previous studies from Wolf Creek (e.g. Carey & Woo, 1998; Lewkowicz & Ednie, 2004).

Halfway up the north-facing slope, there is a 40 m wide highly resistive unit which we believe is a block of sporadic permafrost. Resistivity values are higher than the surrounding slope (> 3810 Ωm) suggesting a higher concentration of ice. Further upslope directly behind the sporadic permafrost block, there is an area of low resistivity (950-1500 Ωm) which could be an area of frozen ground that has a higher fraction of liquid water. Similar to the east-west transect, there is a visible contact line approximately 10 m depth from the ground surface, that could represent where the bedrock begins.

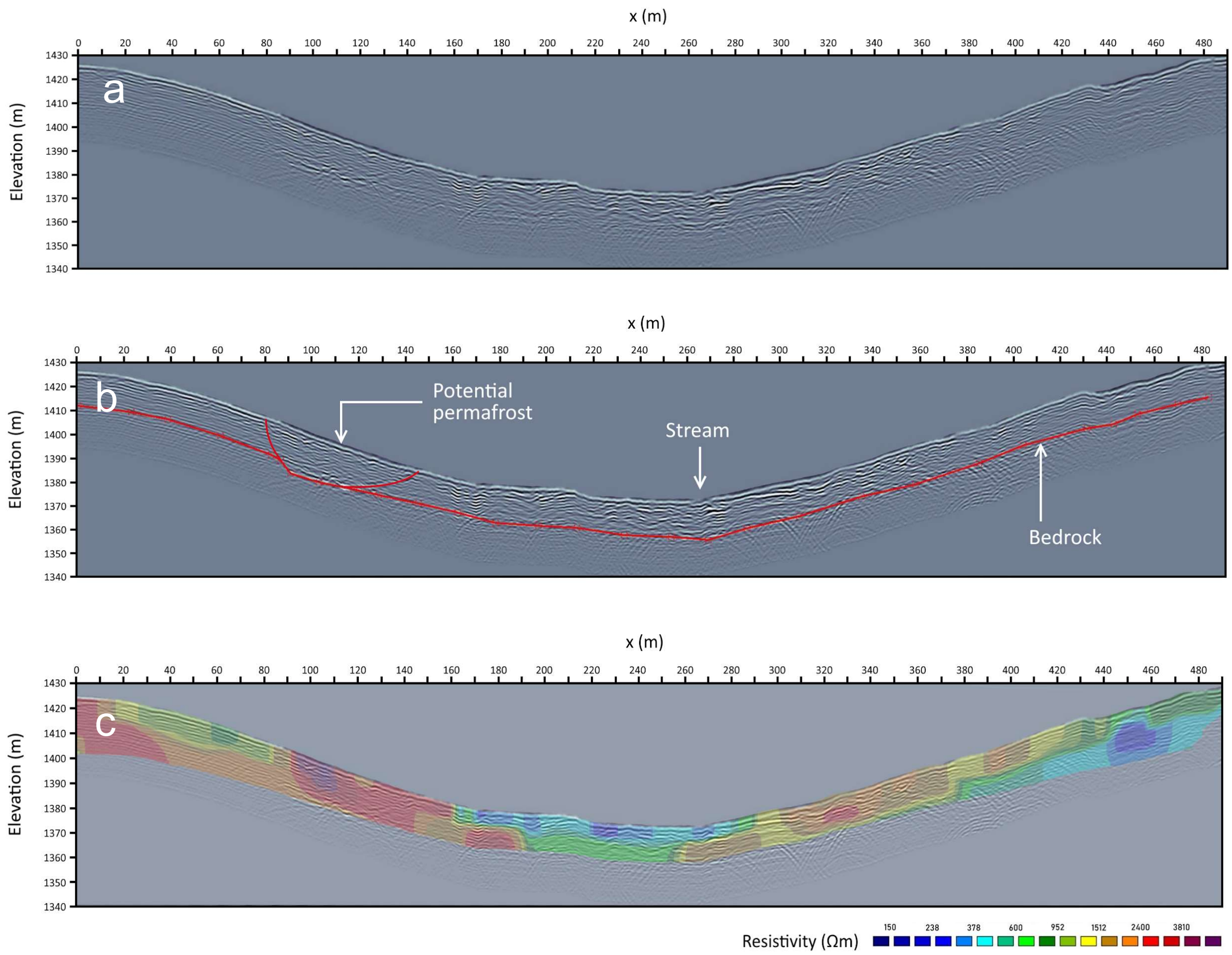

Figure 8. Results from geophysical surveys; (a) results from GPR survey, (b) annotated results from GPR survey, with potential permafrost and bedrock locations marked, (c) combined GPR and CCR results.

The GPR results were integrated with the CCR surveys to validate the geologic and permafrost distribution maps (Figure 8c). The surveys produced GPR results up to a depth of approximately 30 m. On the north-facing slope, a domain that corresponds to the size and location of our suspected sporadic permafrost was detected. We identified two primary reflective surfaces (Figure 8b). One surface was constant at approximately 10-15m depth, which we interpret to be bedrock. The second strong reflection corresponded to the permafrost block from the CCR data, which confirms the presence of frozen ground at that location.

5.2 Model Results

Using SUTRA-ice, multiple simulations with different configurations of sporadic permafrost blocks and climate scenarios were run to identify the impacts of sporadic permafrost on the Granger Creek hydrograph. A conceptual understanding of the shallow groundwater flow system was developed by analyzing different spatial and temporal model outputs such as groundwater exfiltration, pressure, water and ice saturation of individual elements, and the volume of ice in the model. The impacts of sporadic permafrost location are analyzed by comparing the results from the different combinations of three different sporadic permafrost block locations as described above. When analyzing patterns induced by the sporadic permafrost blocks, a seasonal pulse (above summer baseflow) of groundwater exfiltration is observed for all scenarios between September and February, depending on the sporadic permafrost block configuration. It will be referred to as the "spill event", which will be the primary focus of the analysis.

5.2.1 Model Comparison to Field Data

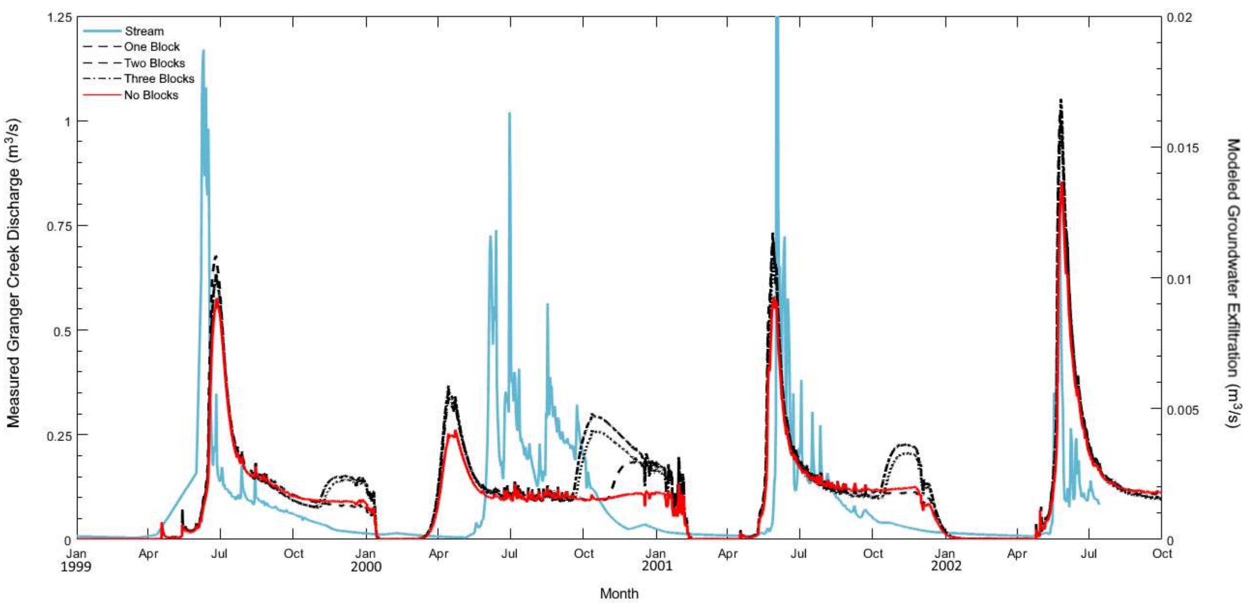

Figure 9. Simulated groundwater exfiltration results with different block configurations (black and red) versus actual stream discharge data from Granger Basin (light blue). NOTE the two datasets are on different scales.

Historically, Granger Basin has not had groundwater wells deeper than 1 meter; therefore, there is not enough data to calibrate the model to measured hydraulic heads. Thus, I set out to design an archetypal model that uses simplified assumptions rather than site-specific parameters (e.g., Zipper *et al.,* 2018).

To test if model outputs were realistic, I compared the simulated groundwater exfiltration results from S5 to gauged discharge data from Granger Basin from 1999 to 2002. The time period between July 1998 to January 1999 had very little data so it was not used for this comparison. Figure 9 shows modeled groundwater exfiltration patterns compared to the patterns of the measured stream discharge. For years 1, 3 and 4 the freshet peak for both datasets are within a reasonable temporal range of each other. Years 2 and 3 have peak groundwater discharge occurring slightly before peak stream discharge, which could indicate a more complex relationship among warming ground, thawing seasonal frost, and pre-freshet melt (Carey *et al.*, 2013). No discernable spill events are observable with the stream hydrograph during the summers, though small pulses of discharge can be seen between January and April 2000 and around January 2001. Further analysis of watershed data would be needed to draw any significant conclusions on the source of those slight increases in discharge late in the year.

Though discharge patterns for modeled and measured results do not match precisely, this is expected as watershed dynamics are complex; groundwater and surface water can have different responses to hydrologic events. Additionally, measured data from this time period is sporadic, and parts of the dataset have been estimated and interpolated (Sean Carey, *personal communication*). The model does not overestimate the amount of groundwater exfiltration, showing a reasonable amount of exfiltration relative to stream discharge. To properly evaluate model outputs, a three-dimensional groundwater model along the transect would be needed.

5.2.2 Groundwater Discharge and Storage Patterns

For all five scenarios, groundwater discharge follows a similar pattern; most of the groundwater exfiltration occurs between April and July when the ground thaws and large amounts of recharge enter the model during the spring snowmelt. After freshet, groundwater discharge rates then level off and stay consistent over the summer and decrease to a negligible amount between December and March when recharge stops due to winter conditions. Nearly all groundwater exfiltration is to the stream outlet as opposed to the land surface. The only exception is during the winter when the ground begins to freeze, a small amount groundwater exfiltration occurs at the land surface.

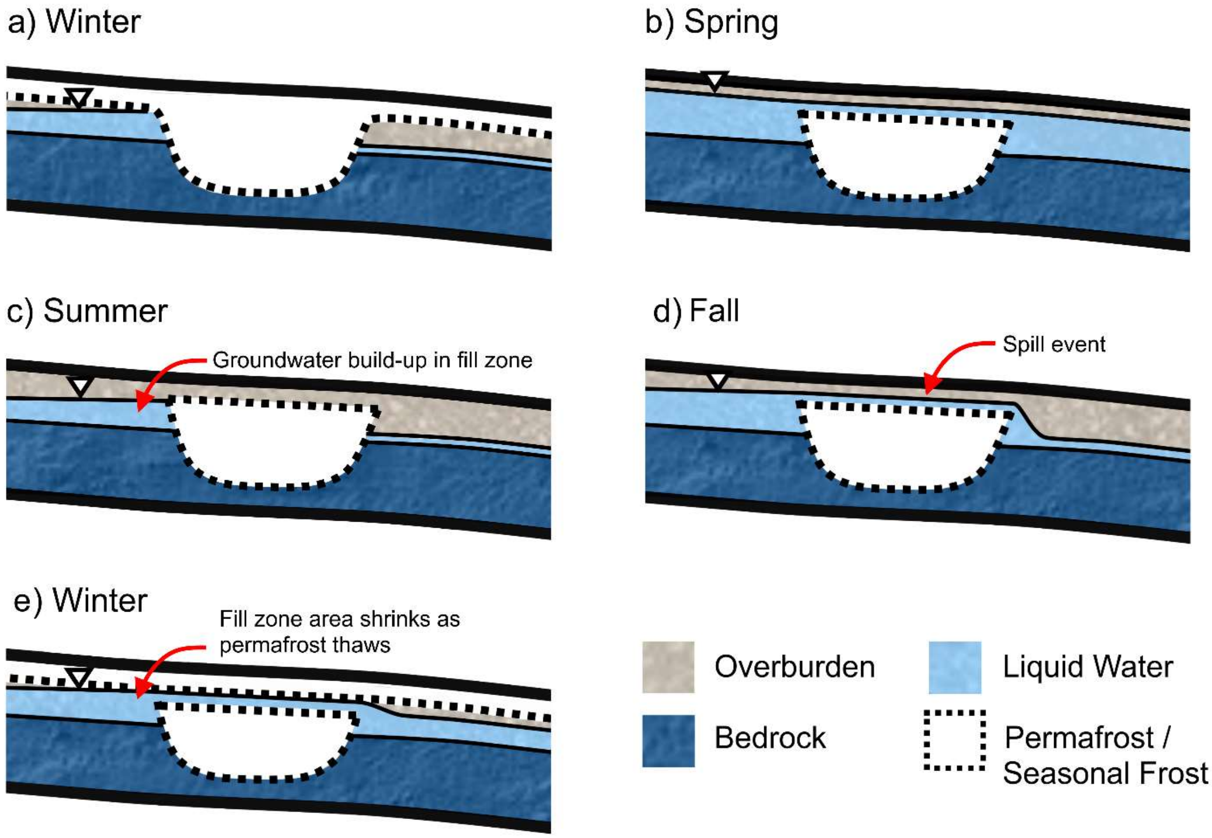

Figure 10. Conceptual diagram of annual discharge patterns as well as fill-spill mechanism; (a) During winter at the start of the simulations, the active layer freezes all the way down to the permafrost block, preventing groundwater flow, (b) When freshet occurs in spring, the water table rises due to increased recharge from snowmelt, (c) After freshet, the sporadic permafrost block prevents groundwater from flowing towards the stream, and it builds up in the "fill zone", (d) Once the "fill zone" reaches a critical threshold, a spill event occurs, typically during fall, (e) Eventually a lateral talik develops over the sporadic permafrost block, allowing water to flow over the block during winter and lessening the effects of the spill in the coming year.

Before the sporadic permafrost blocks completely thaw, a pulse of groundwater discharge to the stream can be observed annually during the fall, between September and February, depending on the sporadic permafrost block configuration (the "spill event", Figure 10). I hypothesize that this is driven via a fill-spill event, where the sporadic permafrost acts as a dam and retains water upslope until a threshold has been reached. Once the water table exceeds the height of the permafrost block, a surge of groundwater spills over the sporadic permafrost and then flows down to the stream. Figure 11 shows the fall spill event over time for the three-block configuration, showing that as the permafrost thaws for scenarios S1-S4 the volume of groundwater discharged during the spill event decreases. I attribute the decrease in spill event magnitude to be due to a smaller 'fill zone' behind the sporadic permafrost block as the active layer thickens over time.

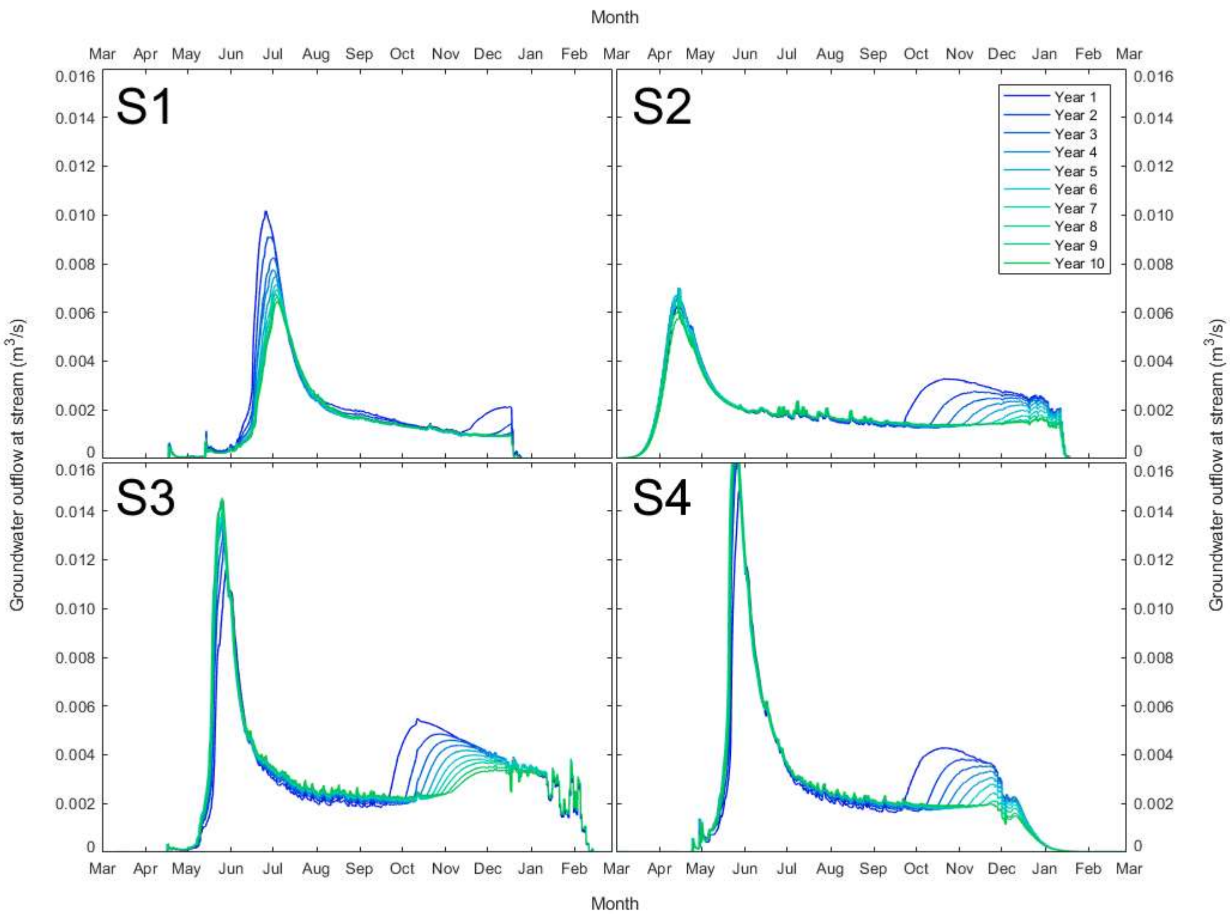

Figure 11. Modeled groundwater exfiltration at the stream for the three-block configuration for the four different climate scenarios. Each figure shows 10 years of model runs with dark blue representing year 1 and light green year 10, highlighting the impact of permafrost thaw on the late fall spill event.

Though the spill event registers on the hydrograph in late fall and sometimes mid-winter, the spill itself typically begins 2-4 months before. For the single-block mid configuration, I use an observation node adjacently downgradient of the sporadic permafrost block to track water saturation which shows the movement of the spill water (

Figure 12). The percent water saturation shows that approximately 2 months after freshet (mid-July) the spill event begins to occur. Water saturation "rapidly" increases to 100% in approximately one month before spilling in mid-August, where saturation continues to decrease until the next year when the next spill event occurs (Figure 13). The spill event is the strongest in the first five years, when saturation reaches 100% during the spill event, but the peak saturation slowly decreases each year as the permafrost thaws. The minimum saturation during winter also increases each year since the thawing of the permafrost allows for a small amount of flow during winter. Around year 25, the spill process is no longer visible and saturation at this node slightly oscillates (e.g. for S3 between 82-88%) depending on the time of year.

Figure 12. Location of the observation node relative to the permafrost block. The observation node sits at the contact of the overburden and bedrock, where the spill occurs.

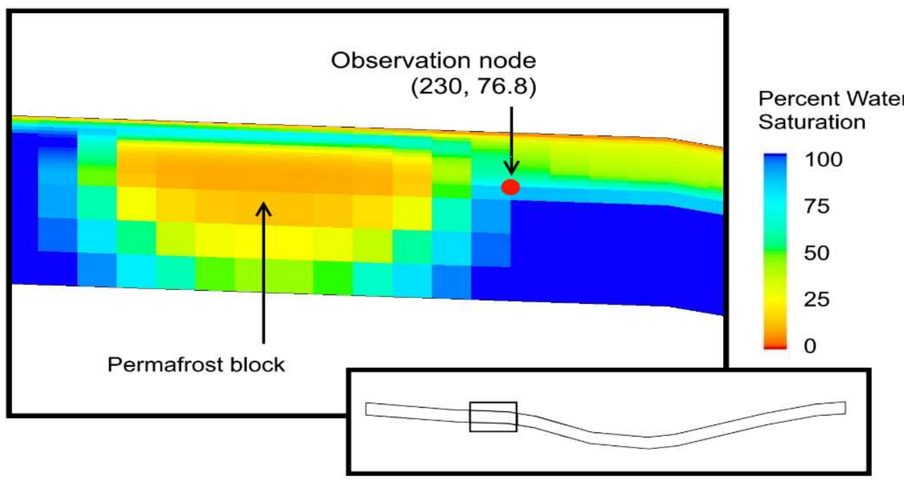

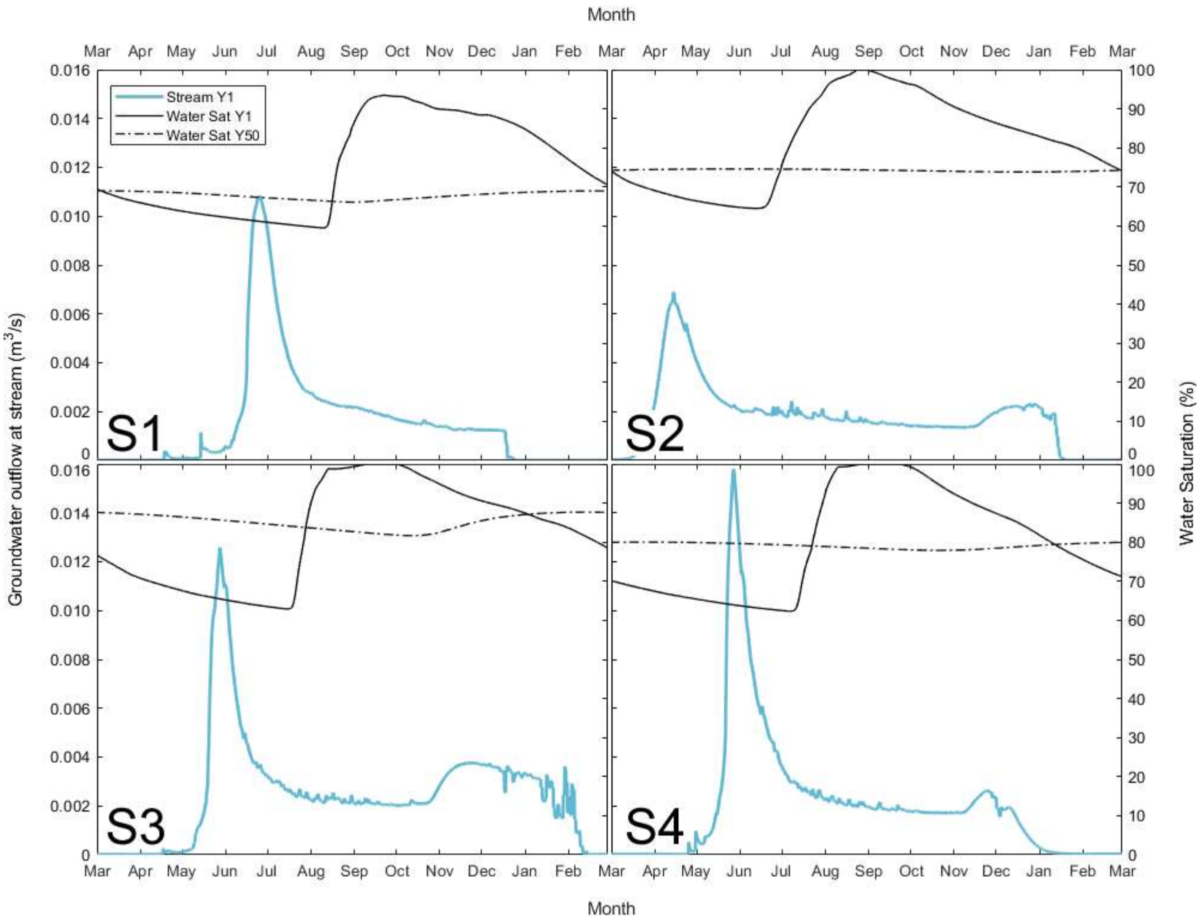

Figure 13. Modeled groundwater exfiltration at stream and liquid water saturation at the observation node (Figure 12) for year 1 (solid line; Y1). For liquid water saturation, the spill event can be seen after freshet during summer months, before the spill registers on the hydrograph in the fall/early winter. The dashed line is included for comparison, showing liquid water saturation for year 50 (Y50), where the permafrost has thawed and there are no more spill events.

When comparing the middle block S3 results to scenarios with less recharge, such as S2, the impacts of the spill and fill are still observed in water saturation. Although there are fewer years with a strong spill (where saturation hits 100%), it takes longer for the spill to occur and reach the stream outlet. For S2, the spill takes 2-3 months to occur, then another 3 months to travel to the stream outlet. The fill-spill process in S2 is likely slower because of the lower transmissivity of the cross-section due to low amounts of recharge entering the model. Similar to S3, it takes about 25 years for the permafrost to thaw and saturation patterns to stabilize, but values only fluctuate between 74-74.5% saturation once it does, showing less variability due to the lower amounts of water entering the system.

For S1, the nature of the spill event differs from the other scenarios due to the low ground temperatures which allow for an increase in the volume of ice over time (

Figure 188). Due to the colder temperatures of S1 and high water table in the "fill zone" behind the sporadic permafrost block, a thin permafrost layer begins to form outwards from the block, creating a "cap" behind the sporadic permafrost block around year 10 (Figure 14). This not only reduces the amount of water that reaches the fill zone, but physically blocks the spill from happening. This dampens both the fill and spill processes, leading to no visible spill in the hydrograph for the mid configuration, and a weak spill for the low configuration (Figure 15).

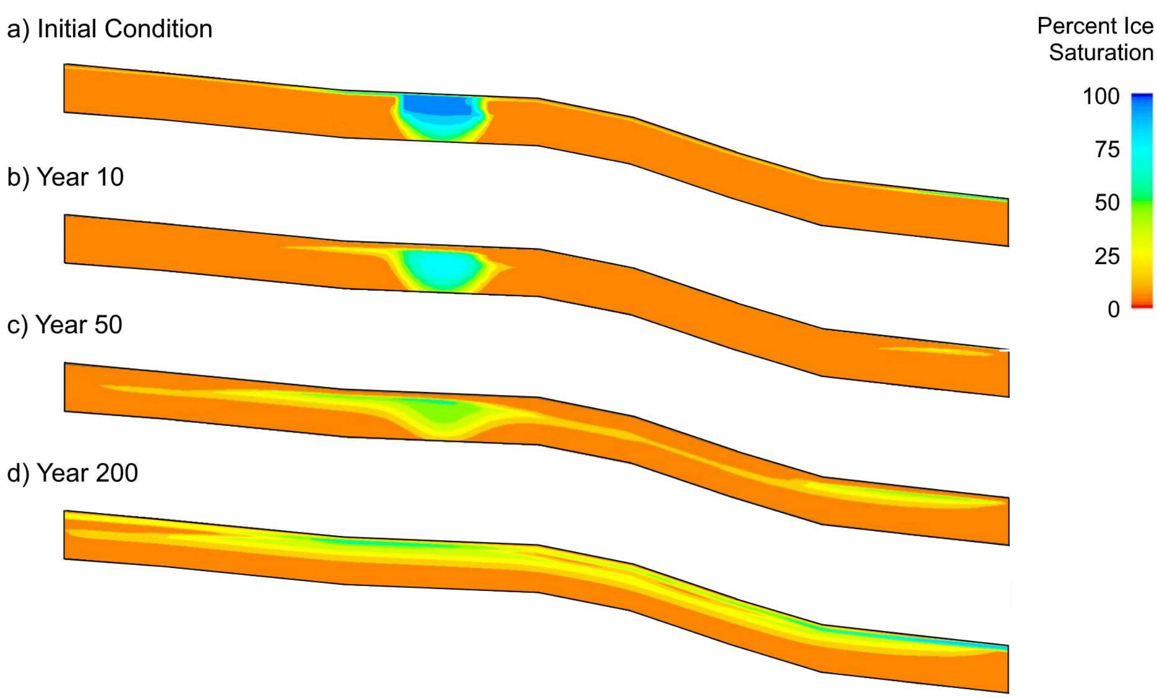

Figure 14. Percent ice saturation of the north facing slope for the mid block configuration in S1. Low ground temperatures and high water table in the "fill zone" leads to an increase in freezing around the sporadic permafrost block around year 10.

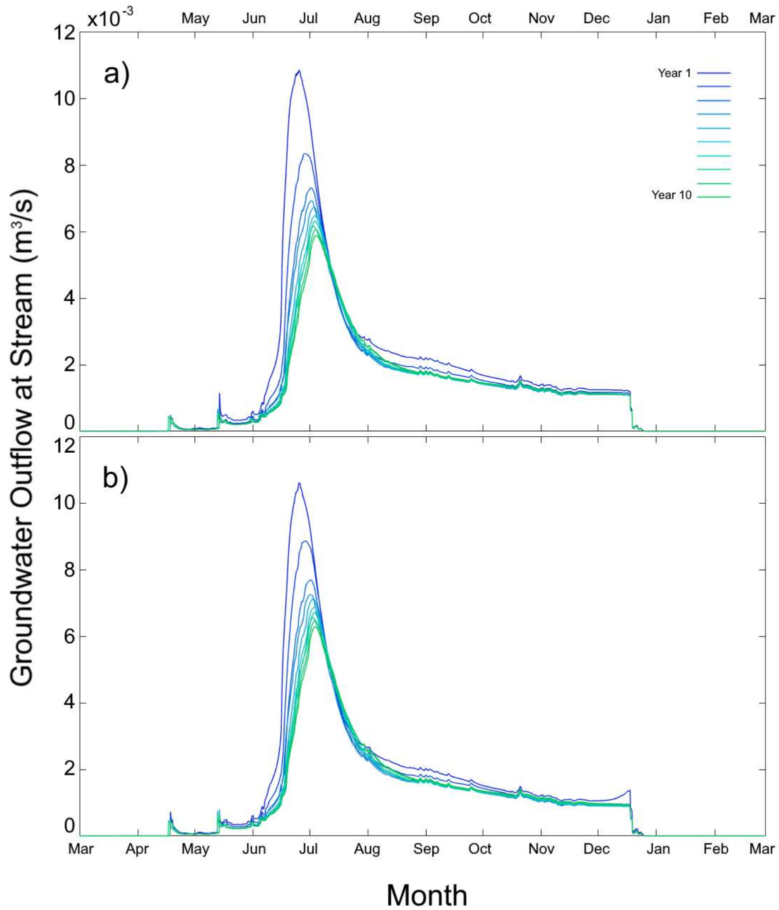

Figure 15. Modeled groundwater exfiltration at the stream for the (a) middle block configuration and (b) low block configuration for S3. Each figure shows 10 years of model runs with dark blue representing year 1 and light green year 10.

5.2.2.1 Impact of Permafrost Distribution

The simulation results show that the closer to the stream the sporadic permafrost block is, the larger the annual spill event. Due to the formation of more permafrost in S1, the impact of the block location is not as significant. For scenarios S2, S3, and S4, the impact of the mid and low sporadic permafrost blocks is apparent regarding the spill event, while the effect of the up block is negligible (Figure 16a). In all three scenarios, the spill event in the low configuration arrives at the stream outlet earlier (1-2 months) due to a shorter travel distance than that of the mid, and releases 13-40% more water as well. In S2 and S4, the permafrost configuration with only the up block exhibits similar patterns to those of the no block configuration during freshet and the spill event, with typically less discharge during freshet compared to mid and low and a lack of spill event. The exception is S3, where during freshet the upper permafrost block configuration produces similar amounts of recharge as the mid and low rather than the no block configuration. In all three scenarios, the mid and low permafrost block locations follow the pattern of higher amounts of discharge during freshet and noticeable spill events later in the year. For the low and mid block configurations, the rate of discharge during the summer between freshet and the spill event is 5-22% lower relative to the no permafrost configuration, before increasing rapidly for the spill event. The groundwater discharge of the up-block configuration remains slightly higher than the no block configuration during this period.

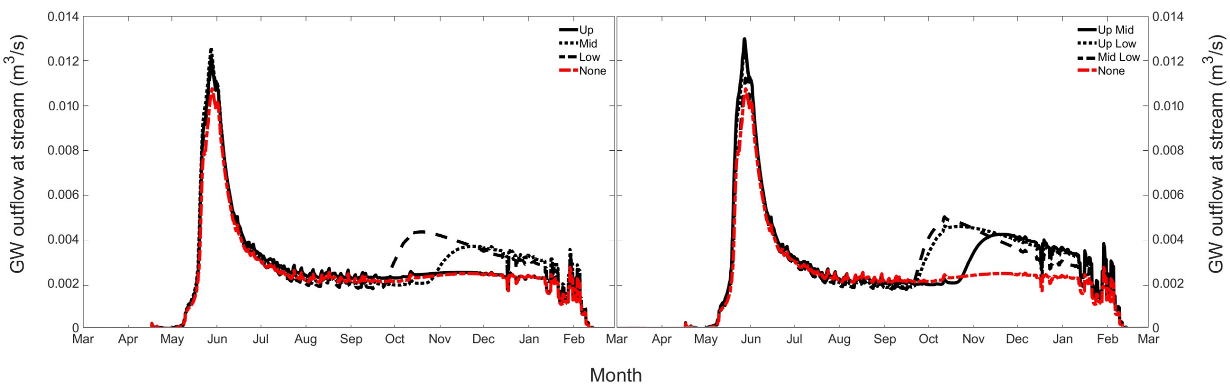

Figure 16. Modeled groundwater exfiltration for (a) the up, mid, and low block simulations compared to the no permafrost simulation, and (b) the up-mid, up-low, and mid-low block simulations compared to the no permafrost simulation. The lower the sporadic permafrost block is, the higher the magnitude of the fill-spill mechanism. For configurations with multiple blocks (b), the lowest block controls the exfiltration pattern.

For S5, spill events are still observed, showing that this process is not unique to the repetitive single year input format of S1-S4. For example, for the three block scenario in S5, years with low recharge have less noticeable spill events, disappearing after the first few years, while years with high recharge still exhibit spill events 16 years after the start of the simulation (

Figure 17). The S5 exfiltration patterns closely follow those of S1-S4, where the spill is strongest with the low block or combinations including the low block, noticeable with the mid block configuration, and not very visible with just the up block.

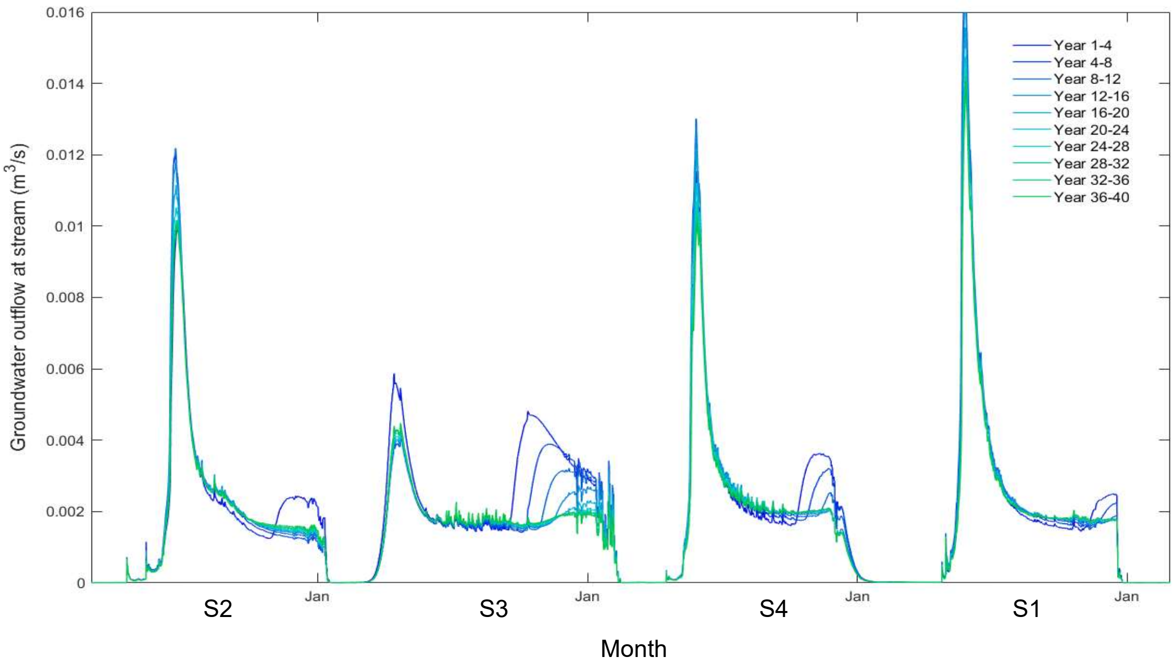

Figure 17. Modeled groundwater exfiltration patterns for the three-block configuration for S5. The figure displays 40 years of model runs in clusters of four, with dark blue representing years 1-4 and light green years 36-40. The S5 simulations show that the spill event is still visible with multiple years of climate inputs.

5.2.2.2 Impact of Number of Permafrost Blocks

Increasing the number of permafrost blocks to two or more generally amplifies the effect of the sporadic permafrost on groundwater discharge (i.e. exfiltration) patterns on the annual hydrograph (Figure 16b). The location of the lowest permafrost block controls the discharge pattern due to the shorter travel time for the spill. The spills induced by upslope blocks cascade into the “fill zone” of the downslope ones, but due to differences in spill timing they do not register as separate exfiltration events. Rather, the additional upslope groundwater adds to the spill event that is already occurring, creating a “fill-cascade” event. Increasing the number of blocks typically decreases the amount of discharge during freshet and increases the amount of discharge during the spill event due to more water being retained by the sporadic permafrost in the fill zones. For S1, the spill effect is more evident with more blocks. The low block does create a very slight spill effect during the first few years before the thin permafrost layer begins to form. When the low and mid block are combined, the spill effect is 44% higher in the first year and 17% higher in the second year of the in the simulated exfiltration hydrograph.

5.2.3 Long-term Permafrost Thaw Patterns

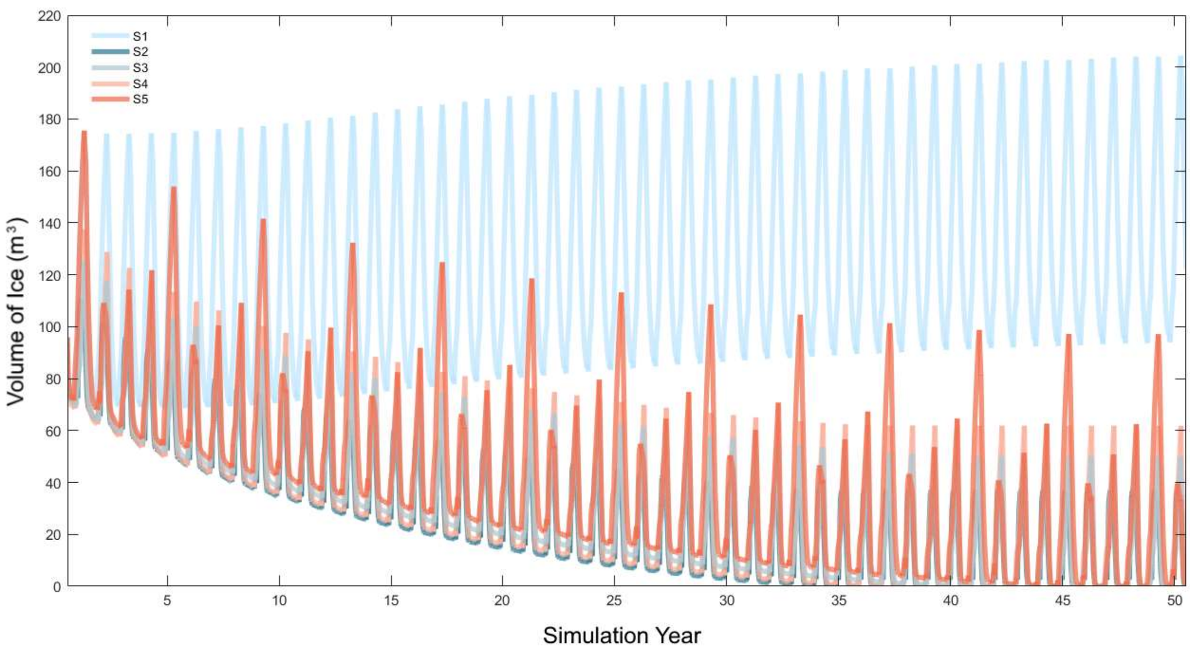

Figure 18. Volume of ice over the entire cross section for the mid block configuration. S2-S5 lose permafrost in 35-45 years, while S1 develops more permafrost.

The volume of pore ice in the five scenarios (S1-S5) shows annual variability as expected due to seasonal freezing. S2-S5 show a gradual decline in the total amount of ice, while the ice in S1 shows the extent of pore-ice and permafrost increasing. Except for S1, annual temperature scenarios showed a decrease in the total annual volume of ice throughout the simulations, with eventual complete thaw during the summer and seasonal frost in the winter. For S1, the low average annual initial temperature regime allows for permafrost forming conditions. For scenarios S2 through S5, summer becomes permafrost free after 35 to 45 years for all permafrost block combinations (

Figure 18).

In order to assess the impact of heat advection as a driver of sporadic permafrost thaw, I compare simulations in which energy transport is only by conduction versus by mixed conduction and advection. Conduction-only simulations are run by setting the permeability everywhere in the model domain to a very low value (1 x 10^{-40} m/s). The simulation results show that advection has only a minor role in the thawing of the permafrost blocks. For example, for S5, when conduction is the only mechanism for heat transfer the disappearance of summer ice occurs 45 to 50 years after the start of the simulation, and for most initial permafrost distributions cases removing advection delays total permafrost thaw by approximately 5-10 years.

5.2.4 North Versus South Facing Slopes

The hydrogeologic differences between the north and south facing slopes using the mid permafrost block configuration are evident in viewing graphical model output (e.g. the ModelViewer visualization tool; Hsieh and Winston, 2002) for all five scenarios. Because the inputs for the surface temperature flux and recharge were different, the two slopes have different temperature regimes and hydrologic responses. Due to the wider range of ground surface temperatures on the south facing slope, temperatures fluctuate more than they do on the north-facing slope. The slope is warmer, with the bedrock layer remaining at 2-3 °C (except S1 which was between 1-2 °C). The north-facing slope is colder in general with the lower overburden and bedrock temperatures are consistently around 0.5-1.0 °C for S2-S5 and between -1.0 and 1.0 °C for S1, with less temperature fluctuations between summer and winter than the south-facing slope. Adding additional sporadic permafrost blocks did not significantly change these values.

When comparing the modeled annual hydrograph of groundwater exfiltration against the model recharge inputs and the measured stream outflow data from Granger Basin, peak groundwater exfiltration occurs right before a majority of the surface recharge enters the model, and slightly before the peak flow from the gauged stream data. These offsets in timing suggests that a majority of groundwater exfiltration during freshet is pre-event water, which is supported by previously Granger Basin research. Mixed methods have shown that a majority of freshet stream discharge is usually pre-event water that resided in the catchment before melt rather than new event water (Carey and Quinton, 2004; Carey *et al.*, 2013; Piovano *et al.*, 2019).

Due to the timing, I hypothesize that groundwater exfiltration is controlled by surface ground thaw and temperature rather than the timing of the recharge input. During winter, the water table near the stream rises as groundwater flows downslope and has no outlet due to the frozen stream (Figure 19). The warmer temperature regime of the south-facing slope allows it to thaw faster and once it does, the groundwater discharges out the north side of the stream. Water continues to exit through this model node until the rest of the model thaws. This suggests that freshet exfiltration is in part controlled by ground temperatures around the stream, in addition to the physical displacement of water during freshet. It is important to note that the process outlined here refers to the deeper groundwater system, not the shallow organic layer within the top meter of the overburden that is described in the literature.

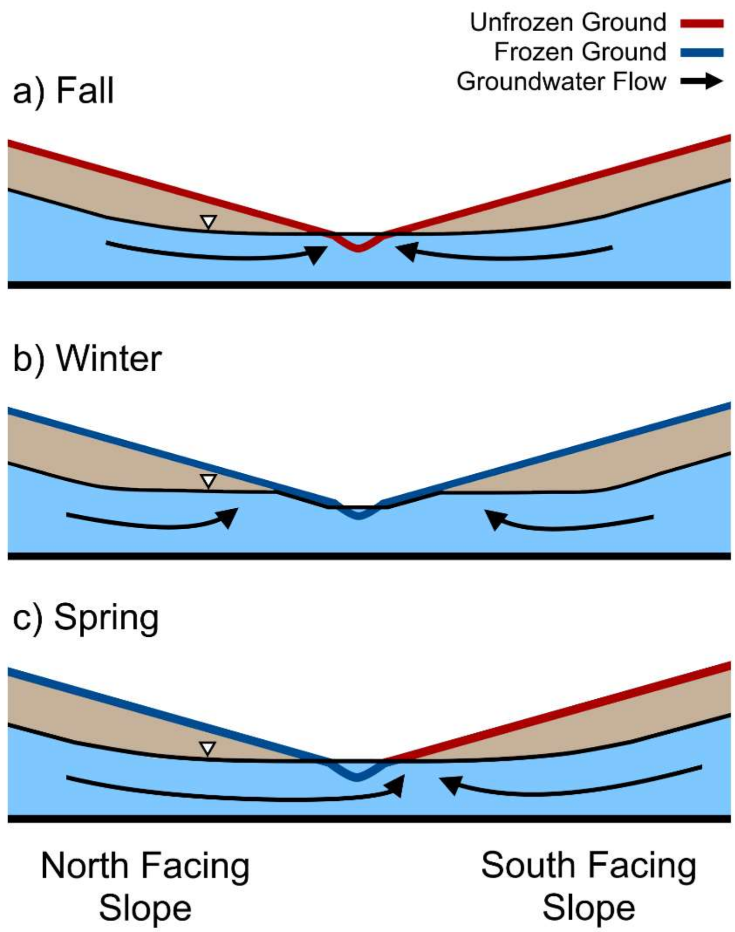

Figure 19 Conceptual diagram of groundwater exfiltration during freshet; (a) in fall, the ground surface is above 0 °C and groundwater exfiltrates to the stream, (b) in winter, the ground freezes which causes the water table to rise, (c) the south facing slope thaws first, giving the stored groundwater an outlet

During winter, the south-facing slope has seasonal frost, with a freeze depth of approximately 3 m for S2-S5 and 5 m for S1. Freezing patterns for the north-facing slope of S1 are discussed above (Figure 14). For S2-S5, the north-facing slope eventually becomes dominated by seasonal frost after the complete thawing of the sporadic permafrost block. Initially the ground freezes down to the top of the sporadic permafrost block, but after 2-6 years, the top of the sporadic permafrost block has thawed downward enough that the two no longer connect in the winter (ice saturation between the seasonal frost and permafrost block is less than 10%). The formation of this lateral talik, between seasonal freezing and top of permafrost, has also been simulated in other settings, and is a pathway through which groundwater can flow through winter (Lamontagne-Hallé *et al.*, 2018). Once this situation develops, the ground freezes to a depth of approximately 3 m each year. This enables year-round flow towards the stream, which causes more water to build up under the frozen stream and may explain the higher amount of discharge during freshet and less pronounced spill event as the years go on even though the sporadic permafrost block is still present.

5.2.5 Sensitivity Analysis Results

To test the effect of the selected parameterization on our model results, a sensitivity analysis was applied to the mid block configuration, comparing the average discharge rate on August 1st, after the freshet event, and December 10th, during the spill event, for year 5 of S3. To compare results, I use a spill estimation index (SEI), which is the ratio of the discharge on December 10th to that of August 1st, allowing quantification of the occurrence and magnitude of the spill event. For S3, December 10th represents the date where the spill is occurring, while August 1st is typically after freshet where discharge is average. I use the SEI and total annual discharge of year 5 to quantify the impact of block location, as well as the permafrost block thickness and model permeability relative to the mid configuration sporadic permafrost block. Results were plotted to visually verify discharge patterns.

Table 3 documents the sensitivity analysis results and shows the percent change in discharge for August 1st and December 1st as well as the SEI and change in SEI relative to groundwater exfiltration of the middle-block permafrost configuration. Permeability values are listed in order of overburden and then bedrock. The middle transition layer is always one magnitude smaller than the overburden.

Table 3. Sensitivity analysis results. Table shows the percent change in discharge for August 1st and December 1st as well as the Spill Estimation Index (SEI) and change in SEI relative to groundwater exfiltration of the middle-block permafrost configuration. Permeability values are listed in order of overburden and then bedrock. The middle transition layer is always one order of magnitude smaller than the overburden.

Parameter	Perturbation	01-Aug Change	10-Dec Change	SEI	SEI Change
Block location	Up block	13%	-21%	0.9808	-28%
	Low block	-4%	0%	1.4116	4%
Permafrost block thickness	2 m thinner	0%	0%	1.3401	-1%
	1 m thinner	0%	0%	1.3495	-1%
	0.5 m thinner	0%	0%	1.3538	0%
	2 m thicker	0%	0%	1.372	1%
	7 m thicker	0%	0%	1.3867	2%
Permeability	High (10^{-9} 10^{-17} m^2)	771%	364%	0.7305	-46%
	High (10^{-10} 10^{-16} m^2)	96%	67%	1.1697	-14%
	High OB (10^{-10} 10^{-18} m^2)	96%	67%	1.1809	-13%
	High BR (10^{-11} 10^{-19} m^2)	-4%	12%	1.6285	20%
	High OB/Low BR (10^{-10} 10^{-19} m^2)	58%	42%	1.2112	-11%
	Low (10^{-13} 10^{-19} m^2)	58%	-24%	0.6686	-51%
	Low OB (10^{-12} 10^{-18} m^2)	63%	0%	0.8333	-39%
	Low BR (10^{-11} 10^{-13} m^2)	33%	-24%	0.7732	-43%
	Low BR (10^{-11} 10^{-15} m^2)	-4%	12%	1.6096	18%
	Low OB/High BR (10^{-12} 10^{-16} m^2)	58%	-3%	0.8357	-39%
	Low OB/High BR (10^{-13} 10^{-15} m^2)	50%	-27%	0.6722	-51%
	Low OB/High BR (10^{-13} 10^{-17} m^2)	50%	-27%	0.6733	-50%
	Low OB/High BR (10^{-15} 10^{-17} m^2)	-81%	-91%	0.6692	-51%

5.2.5.1 Permeability

The model sensitivity to different combinations of permeability for the overburden and bedrock were compared. The simulations experimented with making the overall model more or less permeable, as well as changing the individual layers (i.e. lower permeability overburden and higher permeability bedrock or holding the permeability constant for the overburden and decreasing it for the bedrock; Table 3). For a majority of the permeability configurations, a spill event still occurs though there are variations on the volume of spill and the shape of the hydrograph.

For the overburden, high permeability led to very large increases in groundwater exfiltration due to large amounts of water entering and exiting at the Granger Creek specified pressure nodes to maintain stability. For the most extreme case (overburden permeability of 10^{-9} m^2), there was a 470% increase in annual exfiltration compared to the regular permeability due to the failure of the stream pressure boundary condition under such low permeability. For configurations with low permeability overburden (i.e. 10^{-15} m^2), there was little exfiltration, with 91% less annual discharge. For the scenario with high bedrock permeability (10^{-13} m^2), the permafrost block thawed very rapid due to increased groundwater movement below the block. In this case, there was no spill event and the volume of groundwater exfiltration declined linearly after freshet. For some events with low overburden, there were still spill events even though they had low SEI values. This is because the decline of groundwater exfiltration rates from the freshet events was a gradual linear decay rather than a sudden drop like our base case (Figure 20. Sensitivity analysis of modeled groundwater exfiltration for three permeability values.). This led to a higher average discharge on August 1st, lowering the SEI. If the overburden permeability was too low, (i.e. 10^{-13} m^2), the spill effect was lost.

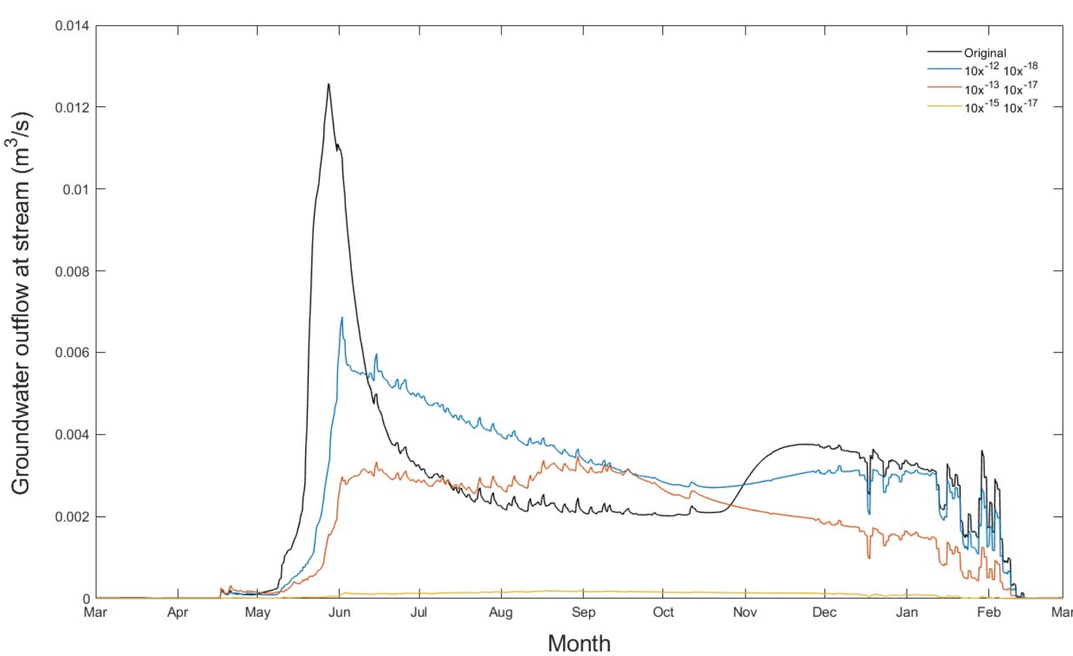

Figure 20. Sensitivity analysis of modeled groundwater exfiltration for three permeability values.

5.2.5.2 Sporadic Permafrost Block Depth

This study assumed that the bottom of the permafrost blocks ended at the top of bedrock. The sensitivity analysis tested if this assumption had an impact on model outcomes. Five variations on the 7 m thickness were used: 5 m, 6 m, 6.5 m, 9 m and 14 m. The thickness variations were constrained by the downward coarsening of the model's discretization layers. The results showed that the thickness of the permafrost itself did not alter the presence of the spill event but impacted the intensity of the event and how many years the event continued to occur for. The initial years showed very little difference in the timing and intensity of the spill event among the different thicknesses, but as the permafrost blocks thawed, the simulations with thinner blocks had smaller spill events compared to those with thicker blocks. SEI values for all five simulations were very similar to that of the base case, with the percent change varying from 0-2%, showing there was not a significant difference in the ratio between the early fall and early winter discharge, and that a spill was still present for these different block depths. These results indicate that the spill event is controlled by the thickness of the active layer, which means that most water is flowing over the permafrost block rather than below it.

5.2.5.3 Sensitivity Analysis Discussion

The results of the sensitivity analysis show that there are a range of values for which the spill can happen. Location of the permafrost block along the slope and permeability have the largest impact on the likelihood of a spill event. For permeability, values that are too high or too low cause too much or too little groundwater flow, and these permeability values are not representative of the typical composition of these settings. The general range where spill occurs is between 1×10^{-10} to 10^{-12} m^2 for overburden permeability and a maximum of 1×10^{-15} m^2 for bedrock. For the sporadic permafrost thickness, the depth that the permafrost reaches is less important because the controlling factor is the thickness of the active layer.

6 Conclusion

This thesis used a combination of field data and numerical modeling to develop a conceptual understanding of groundwater processes in a mountain headwater catchment underlain by sporadic permafrost. Groundwater processes in these mountain catchments are not well studied, and more research is needed to better understand the processes that control baseflow generation. As air temperatures continue to rise and precipitation patterns change (Bintanja and Andry, 2017), the limits of the discontinuous and continuous permafrost zones will begin to shift due to their sensitivity to temperature and snowpack thickness (Smith and Riseborough, 2002). In western Canada temperatures have been rising, particularly in winter (DeBeer *et al.*, 2016). This work is critical for proper management of northern water resources and understanding processes such as fill-spill can help stakeholders adapt to changing flow regimes induced by climate change.

6.1 Fill-Spill Processes in Hydrology

Fill-spill is a mechanism that controls water movement through a landscape where depressions along a slope must reach their storage capacity before the water "spills" out and continues downslope creating a cascading effect. This process can be observed in a variety of landscapes and on a range of scales, from bedrock microtopography to networks of wetlands.

Fill-spill processes have been studied in soil-filled valleys, wetlands, and prairie ponds (Shaw *et al.*, 2012; Connon *et al.*, 2014). In these settings, antecedent moisture and storage conditions drive fill-spill processes which impact the connectivity of a basin during a freshet or storm events, creating a dynamic basin contributing area. Some studies have specifically examined the impact of bedrock topography impact storage and runoff (Spence and Woo, 2003; Tromp-van Meerveld and McDonnell, 2006; Hayashi, 2019). Specific to frozen landscapes, Wright *et al.* (2008) examined fill-spill in the context of frost-table topography, noting that dynamic depressions in the frost table at a forested peat plateau site had an impact on peat thaw as well as runoff generation. Coles and McDonnell (2018) show that fill-spill processes generate snowmelt-runoff over frozen ground before thaw begins in a prairie setting. To the best of my knowledge, there are no studies that describe fill-spill processes in sporadic permafrost environments.

6.2 Fill-Spill Processes at Granger Basin

The field data and model results suggest that fill-spill processes are possible in areas of Granger Basin underlain by sporadic permafrost, but many factors affect how much it influences the annual hydrograph. Lewkowicz and Ednie (2004) indicated there was a 50-90% probability of widespread discontinuous permafrost in the lower half of the Granger Basin watershed where this study takes place. Depending on the configuration of the sporadic permafrost blocks, spill events could be staggered, with different timings and intensity depending on the sporadic block location, proximity to the stream, or the number of blocks.

With the model showing a rapid rate of permafrost thaw under contemporary climate scenarios, the basin could also have significantly less permafrost than previous studies predicted. Due to the model's inability to retain the sporadic permafrost block or form new permafrost in scenarios S2-S5, we assume that the climate at Granger Basin has already entered a 'thaw mode', indicating that system is well out of equilibrium and will continue to rapidly thaw. The simulations indicate that modern climate regimes at Granger Basin could be too warm to maintain sporadic permafrost, and that the north facing slope could soon only have seasonal frost. This research also shows that the timing and intensity of groundwater exfiltration throughout the year will change as permafrost continues to thaw.

6.3 Model Improvements and Future Studies

While this research provides some evidence of how sporadic permafrost may impact groundwater exfiltration, there are improvements that can increase the accuracy of our model as well as uncover more about groundwater processes in these regions. In a watershed with little groundwater data like Granger Basin, calibrating and increasing accuracy can be difficult but the quality of boundary conditions can be improved. Integrating a surface-energy balance or snowpack model may improve the timing and accuracy of snowmelt recharge into the model, which can give a more insightful look into freshet groundwater processes. Additionally, a surface-energy balance model would improve the model's ability to calculate surface temperature, which is useful if shallow soil temperature data are not available. When incorporating field data, rather than having one set of data represent each slope (in this case soil temperature, snowpack thickness, and precipitation), multiple datasets representing multiple segments of the cross-section may produce more realistic results. Air temperatures can range greatly by elevation from the valley to the edges of the watershed, and environmental factors such as vegetation and wind have significant impacts on snowpack formation and ground temperatures which can lead to snowmelt happening at different times across the basin (Dornes *et al.*, 2006; McCartney *et al.*, 2006; Marsh *et al.*, 2012). Differing snowmelt times geospatially could affect peak groundwater exfiltration; where this study assumed one snowmelt event that occurred rapidly on each slope, multiple staggered snowmelt events along the slope might impact on the hydrograph and fill-spill processes. To better understand the relationship between ground surface temperature and freshet baseflow contribution, more simulations using a wider range of temperatures and recharge volumes along our surface boundary condition are needed.

To better understand the dynamic groundwater processes occurring in mountain headwater catchments, multiple aspects of the numerical model can be further developed for future studies. For this study, the surface recharge boundary is based on field precipitation data. Using values from literature, a given percentage of rainfall and snowmelt becomes recharge to the subsurface. Using this method, more sensitivity analyses using different percentages of precipitation and snowmelt for recharge could give insight on the range of climate scenarios fill-spill could occur under. Some modeling studies use a constant rate of recharge for each season (Lamontagne-Hallé *et al.*, 2018), so it would be interesting to see if fill-spill events can still occur under those scenarios, or if it's a function of individual precipitation and snowmelt events. Additionally, evaluating the impact of sporadic permafrost blocks in additional locations and experimenting with the impacts of slope angle could yield more nuanced results.

Previous fill-spill studies have observed the process occurring on surfaces in three dimensions with depressions, whereas in this study the fill spill is induced by the permafrost acting as a barrier on a 2-D cross-section. This raises questions about the lateral extent of sporadic permafrost blocks, and the role of transverse or lateral flow in permafrost induced fill-spill. To investigate this, SUTRA's 3-D modeling capabilities could be used. Meerveld and Weiler (2008) show that their fill-spill model accuracy increased with the inclusion of bedrock leakage, which suggests a similar process could also be occurring.

Future experiments comparing results from simulations using the entire cross-section versus just the north or south facing slope would allow more insight into processes occurring on each slope. By running simulations with just the north facing slope, I can analyze the impact of the earlier ground thaw on the south facing slope, and its impacts regarding groundwater exfiltration during freshet. In studying the peak groundwater discharge during snowmelt, a warming rate applied to the different climate scenarios may also provide more insight on the sensitivity of peak discharge timing to ground thaw. To test the results of our 2-D model, groundwater monitoring wells should be installed at the contact of the overburden and bedrock upslope from the anticipated location of the sporadic permafrost at Granger Basin in the "fill zone". To examine if spilling occurs, water level data from the predicted fill site would provide information on the timing and possible thresholds that induce spill events. This would also help calibrate the model for future applications and provide valuable insight on the accuracy of our understanding of groundwater processes at Granger Basin.

8 References

Angelopoulos MC, Pollard WH, Couture NJ. 2013. The application of CCR and GPR to characterize ground ice conditions at Parsons Lake, Northwest Territories. *Cold Regions Science and Technology* **85**: 22–33 DOI: 10.1016/j.coldregions.2013.10.003

Annan AP. 2005. 11. Ground-Penetrating Radar. In *Near-Surface Geophysics*Society of Exploration Geophysicists; 357–438. DOI: 10.1190/1.9781560801719.ch11

Bense VF, Ferguson G, Kooi H. 2009. Evolution of shallow groundwater flow systems in areas of degrading permafrost. *Geophysical Research Letters* **36** (22): L22401 DOI: 10.1029/2009GL039225

Bense VF, Kooi H, Ferguson G, Read T. 2012. Permafrost degradation as a control on hydrogeological regime shifts in a warming climate. *Journal of Geophysical Research: Earth Surface* **117** (F3): n/a-n/a DOI: 10.1029/2011JF002143

Bintanja R, Andry O. 2017. Towards a rain-dominated Arctic. *Nature Climate Change* **7** (4): 263–267 DOI: 10.1038/nclimate3240

Boucher JL, Carey SK. 2010. Exploring runoff processes using chemical , isotopic and hydrometric data in a discontinuous permafrost catchment: 508–519 DOI: 10.2166/nh.2010.146

Briggs MA, Walvoord MA, McKenzie JM, Voss CI, Day-Lewis FD, Lane JW. 2014. New permafrost is forming around shrinking Arctic lakes, but will it last? *Geophysical Research Letters* DOI: 10.1002/2014GL059251

Brown J, Ferrians OJJ, Heginbottom JA, Melnikov ES. 1998. Circum-Arctic Map of Permafrost and Ground-Ice Conditions.

Cairns DW. 2014. Simulation of groundwater flow in mountain watersheds.University of Lethbridge.

Callaghan T V., Johansson M, Brown RD, Groisman PY, Labba N, Radionov V, Barry RG, Bulygina ON, Essery RLH, Frolov DM, et al. 2011. The changing face of arctic snow cover: A synthesis of observed and projected changes. *Ambio* **40** (SUPPL. 1): 17–31 DOI: 10.1007/s13280-011-0212-y

Carey SK, Quinton WL. 2004. Evaluating snowmelt runoff generation in a discontinuous permafrost catchment using stable isotope , hydrochemical and hydrometric data *. (August 2003): 25–29

Carey SK, Woo M. 1998. Snowmelt Hydrology of Two Subarctic Slopes, Southern. *Nordic Hydrology* **29**

Carey SK, Woo M. 2001. Slope runoff processes and ¯ ow generation in a subarctic , subalpine catchment. **253**

Carey SK, Boucher JL, Duarte CM. 2013. Inferring groundwater contributions and pathways to stream fl ow during snowmelt over multiple years in a discontinuous permafrost subarctic environment (Yukon , Canada). *Hydrogeology Journal* **21**: 67–77 DOI: 10.1007/s10040-012-0920-9

Clilverd HM, White DM, Tidwell AC, Rawlins MA. 2011. The Sensitivity of Northern Groundwater Recharge to Climate Change: A Case Study in Northwest Alaska1. *JAWRA Journal of the American Water Resources Association* **47** (6): 1228–1240 DOI: 10.1111/j.1752-1688.2011.00569.x

Coles AE, McDonnell JJ. 2018. Fill and spill drives runoff connectivity over frozen ground. *Journal of Hydrology* **558**: 115–128 DOI: 10.1016/j.jhydrol.2018.01.016

Connon RF, Quinton WL, Craig JR, Hayashi M. 2014. Changing hydrologic connectivity due to permafrost thaw in the lower Liard River valley, NWT, Canada. *Hydrological Processes* **28** (14): 4163–4178 DOI: 10.1002/hyp.10206

DeBeer CM, Wheater HS, Carey SK, Chun KP. 2016. Recent climatic, cryospheric, and hydrological changes over the interior of western Canada: a review and synthesis. *Hydrology and Earth System Sciences* **20** (4): 1573–1598 DOI: 10.5194/hess-20-1573-2016

Déry SJ, Hernández-Henríquez MA, Burford JE, Wood EF. 2009. Observational evidence of an intensifying hydrological cycle in northern Canada. *Geophysical Research Letters* **36** (13): L13402 DOI: 10.1029/2009GL038852

Dornes PF, Pomeroy JW, Pietroniro A, Carey SK, Quinton WL. 2006. The Use of Inductive and Deductive Reasoning to Model Snowmelt Runoff from Northern Mountain Catchments. In *International Congress on Environmental Modelling and Software*.

Dornes PF, Pomeroy JW, Pietroniro A, Carey SK, Quinton WL. 2008. Influence of landscape aggregation in modelling snow-cover ablation and snowmelt runoff in a sub-arctic mountainous environment. *Hydrological Sciences Journal* **53** (4): 725–740 DOI: 10.1623/hysj.53.4.725

Evans SG, Ge S. 2017. Contrasting hydrogeologic responses to warming in permafrost and seasonally frozen ground hillslopes. *Geophysical Research Letters* **44** (4): 1803–1813 DOI: 10.1002/2016GL072009

Forster C, Smith L. 1988. Groundwater flow systems in mountainous terrain: 2. Controlling factors. *Water Resources Research* **24** (7): 1011–1023 DOI: 10.1029/WR024i007p01011

Frampton A, Painter SL, Destouni G. 2013. Permafrost degradation and subsurface-flow changes caused by surface warming trends. *Hydrogeology Journal* **21** (1): 271–280 DOI: 10.1007/s10040-012-0938-z

Ge S, McKenzie J, Voss C, Wu Q. 2011. Exchange of groundwater and surface-water mediated by permafrost response to seasonal and long term air temperature variation. *Geophysical Research Letters* **38** (14): n/a-n/a DOI: 10.1029/2011GL047911

Gorbunov AP. 1978. Permafrost Investigations in High-Mountain Regions, Arctic and Alpine Research. *Arctic and Alpine Research* **10** (2) DOI: 10.1080/00040851.1978.12003967

Grenier C, Anbergen H, Bense V, Chanzy Q, Coon E, Collier N, Costard F, Ferry M, Frampton A, Frederick J, et al. 2018. Groundwater flow and heat transport for systems undergoing freeze-thaw: Intercomparison of numerical simulators for 2D test cases. *Advances in Water Resources* **114**: 196–218 DOI: 10.1016/j.advwatres.2018.02.001

Guodong C, Dramis F. 1992. Distribution of mountain permafrost and climate. *Permafrost and Periglacial Processes* **3** (2): 83–91 DOI: 10.1002/ppp.3430030205

Harris SA, Corte AE. 1992. Interactions and relations between mountain permafrost, glaciers, snow and water. *Permafrost and Periglacial Processes* **3** (2): 103–110 DOI: 10.1002/ppp.3430030207

Harris SA, Giardino JR. 1993. Permafrost in the mountain range of North America. In *Proceedings of the 6th International Conference on Permafrost, Beijing, China*S. China Univ. of Technol. Press: Guangzhou, China.

Hauck C, Kneisel C (eds). 2008. *Applied Geophysics in Periglacial Environments*. Cambridge University Press: Cambridge. DOI: 10.1017/CBO9780511535628

Hayashi M. 2019. Alpine hydrogeology: The critical role of groundwater in sourcing the headwaters of the world. *Groundwater* DOI: 10.1111/gwat.12965

Hsieh P, Winston R. 2002. User's guide to Model Viewer, a program for three-dimensional visualization of ground-water model results DOI: 10.3133/ofr02106

Ishikawa M, Sharkhuu N, Zhang Y, Kadota T, Ohata T. 2005. Ground thermal and moisture conditions at the southern boundary of discontinuous permafrost, Mongolia. *Permafrost and Periglacial Processes* **16** (2): 209–216 DOI: 10.1002/ppp.483

Kurylyk BL. 2019. Engineering challenges of warming. *Nature Climate Change* **9** (11): 807–808 DOI: 10.1038/s41558-019-0612-8

Kurylyk BL, Hayashi M, Quinton WL, McKenzie JM, Voss CI. 2016. Influence of vertical and lateral heat transfer on permafrost thaw, peatland landscape transition, and groundwater flow. *Water Resources Research* **52** (2): 1286–1305 DOI: 10.1002/2015WR018057

Lamontagne-Hallé P, McKenzie JM, Kurylyk BL, Zipper SC. 2018. Changing groundwater discharge dynamics in permafrost regions. *Environmental Research Letters*

Langston G, Bentley LR, Hayashi M, Mcclymont A, Pidlisecky A. 2011. Internal structure and hydrological functions of an alpine proglacial moraine. *Hydrological Processes* **25** (19): 2967–2982 DOI: 10.1002/hyp.8144

Lemieux J-M, Fortier R, Talbot-Poulin M-C, Molson J, Therrien R, Ouellet M, Banville D, Cochand M, Murray R. 2016. Groundwater occurrence in cold environments: examples from Nunavik, Canada. *Hydrogeology Journal* **24** (6): 1497–1513 DOI: 10.1007/s10040-016-1411-1

Lemke P, Ren J, Alley RB, Allison I, Carrasco J, Flato G, Fujii Y, Kaser G, Mote P, Thomas RH, et al. 2007. Observations: Changes in Snow, Ice and Frozen Ground Coordinating. *Climate Change 2007: The Physical Science Basis. Contribution of Working Group I to the Fourth Assessment Report of the Intergovernmental Panel on Climate Change*

Lessels JS, Tetzlaff D, Carey SK, Smith P, Soulsby C. 2015. A coupled hydrologybiogeochemistry model to simulate dissolved organic carbon exports from a permafrost-influenced catchment. *Hydrological Processes* **29** (26): 5383–5396 DOI: 10.1002/hyp.10566

Lewkowicz AG, Ednie M. 2004. Probability mapping of mountain permafrost using the BTS method, Wolf Creek, Yukon Territory, Canada. *Permafrost and Periglacial Processes* **15** (1): 67–80 DOI: 10.1002/ppp.480

Loke MH, Barker RD. 1996. Practical techniques for 3D resistivity surveys and data inversion1. *Geophysical Prospecting* **44** (3): 499–523 DOI: 10.1111/j.1365-2478.1996.tb00162.x

Marsh CB, Pomeroy JW, Spiteri RJ. 2012. Implications of mountain shading on calculating energy for snowmelt using unstructured triangular meshes. *Hydrological Processes* **26** (12): 1767–1778 DOI: 10.1002/hyp.9329

Mccartney SE, Carey SK, Pomeroy JW. 2006. Intra-basin variability of snowmelt water balance calculations in a subarctic catchment. **1016** (June 2005): 1001–1016 DOI: 10.1002/hyp.6125

McCartney SE, Carey SK, Pomeroy JW. 2006. Intra-basin variability of snowmelt water balance calculations in a subarctic catchment. *Hydrological Processes* **20** (4): 1001–1016 DOI: 10.1002/hyp.6125

McGuire AD, Lawrence DM, Koven C, Clein JS, Burke E, Chen G, Jafarov E, MacDougall AH, Marchenko S, Nicolsky D, et al. 2018. Dependence of the evolution of carbon dynamics in the northern permafrost region on the trajectory of climate change. *Proceedings of the National Academy of Sciences* **115** (15): 3882–3887 DOI: 10.1073/pnas.1719903115

Mckenzie JM, Voss CI, Siegel DI. 2007. Groundwater flow with energy transport and water-ice phase change: Numerical simulations, benchmarks, and application to freezing in peat bogs. *Advances in Water Resources* DOI: 10.1016/j.advwatres.2006.08.008

McKenzie JM, Voss CI. 2013. Permafrost thaw in a nested groundwater-flow system. *Hydrogeology Journal* **21**: 299–316 DOI: 10.1007/s10040-012-0942-3

Meerveld I, Weiler M. 2008. Hillslope dynamics modeled with increasing complexity. *Journal of Hydrology* **361** (1–2): 24–40 DOI: 10.1016/j.jhydrol.2008.07.019

Muskett RR, Romanovsky VE. 2009. Groundwater storage changes in arctic permafrost watersheds from GRACE and insitu measurements. *Environmental Research Letters* **4** (4) DOI: 10.1088/1748-9326/4/4/045009

Neal A. 2004. Ground-penetrating radar and its use in sedimentology: principles, problems and progress. *Earth-Science Reviews* **66** (3–4): 261–330 DOI: 10.1016/j.earscirev.2004.01.004

Osterkamp TE. 2005. The recent warming of permafrost in Alaska. *Global and Planetary Change* **49** (3–4): 187–202 DOI: 10.1016/j.gloplacha.2005.09.001

De Pascale GP, Pollard WH, Williams KK. 2008. Geophysical mapping of ground ice using a combination of capacitive coupled resistivity and ground-penetrating radar, Northwest Territories, Canada. *Journal of Geophysical Research: Earth Surface* **113** (2): 1–15 DOI: 10.1029/2006JF000585

Paznekas A, Hayashi M. 2016. Groundwater contribution to winter streamflow in the Canadian Rockies. *Canadian Water Resources Journal / Revue canadienne des ressources hydriques* **41** (4): 484–499 DOI: 10.1080/07011784.2015.1060870

Piovano TI, Tetzlaff D, Carey SK, Shatilla NJ, Smith A, Soulsby C. 2019. Spatially distributed tracer-aided runoff modelling and dynamics of storage and water ages in a permafrost-influenced catchment. *Hydrology and Earth System Sciences* **23** (6): 2507–2523 DOI: 10.5194/hess-23-2507-2019

Pomeroy JW, Brun E. 2001. Physical Properties of Snow. In *Snow Ecology*Cambridge University Press; 859–863. DOI: 10.1007/978-90-481-2642-2_422

Pomeroy JW, Hedstrom N, Parviainen J. 1998. The Snow Mass Balance of Wolf Creek, Yukon: Effects of Snow Sublimation and Redistribution. In *Wolf Creek Research Basin Workshop*.

Reynolds JM. 2011. *An Introduction to Applied and Environmental Geophysics*. Wiley.

Romanovsky VE, Smith SL, Christiansen HH. 2010. Permafrost thermal state in the polar northern hemisphere during the international polar year 2007-2009: A synthesis. *Permafrost and Periglacial Processes* **21** (2): 106–116 DOI: 10.1002/ppp.689

Seguin M-K, Stein J, Nilo O, Jalbert C, Ding Y. 1998. Hydrogeophysical Investigation of the Wolf Creek Watershed, Yukon Territory, Canada. *Proceedings from the Wolf Creek Research Basin: Hydrology, Ecology, Environment workshop, Whitehorse, Yukon*: 55–78

Shaw DA, Vanderkamp G, Conly FM, Pietroniro A, Martz L. 2012. The Fill-Spill Hydrology of Prairie Wetland Complexes during Drought and Deluge. *Hydrological Processes* **26** (20): 3147–3156 DOI: 10.1002/hyp.8390

Shirazi T, Allen DM, Quinton WL, Pomeroy JW. 2009. Estimating soil thaw energy in sub-Alpine tundra at the hillslope scale, Wolf Creek, Yukon Territory, Canada. *Hydrology Research* **40** (1): 1 DOI: 10.2166/nh.2009.043

Sicart JE, Pomeroy JW, Essery RLH, Bewley D. 2006. Incoming longwave radiation to melting snow: observations, sensitivity and estimation in Northern environments. *Hydrological Processes* **20** (17): 3697–3708 DOI: 10.1002/hyp.6383

Slater AG, Lawrence DM. 2013. Diagnosing Present and Future Permafrost from Climate Models. *Journal of Climate* **26** (15): 5608–5623 DOI: 10.1175/JCLI-D-12-00341.1

Smith LC. 2005. Disappearing Arctic Lakes. *Science* **308** (5727): 1429–1429 DOI: 10.1126/science.1108142

Smith MW, Riseborough DW. 2002. Climate and the limits of permafrost: a zonal analysis. *Permafrost and Periglacial Processes* **13** (1): 1–15 DOI: 10.1002/ppp.410

Spence C, Woo M. 2003. Hydrology of subarctic Canadian shield: soil-filled valleys. *Journal of Hydrology* **279** (1–4): 151–166 DOI: 10.1016/S0022-1694(03)00175-6

Tromp-van Meerveld HJ, McDonnell JJ. 2006. Threshold relations in subsurface stormflow: 2. The fill and spill hypothesis. *Water Resources Research* **42** (2) DOI: 10.1029/2004WR003800

Viviroli D, Kummu M, Meybeck M, Wada Y. 2019. Increasing dependence of lowland population on mountain water resources. *EarthArXiv* DOI: 10.31223/osf.io/fr5uj

Voss CI, Provost A. 2002. SUTRA: A model for 2D or 3D saturated-unsaturated, variable-density ground-water flow with solute or energy transport DOI: 10.3133/wri024231

Walvoord MA, Kurylyk BL. 2016. Hydrologic Impacts of Thawing Permafrost—A Review. *Vandose Zone Journal* DOI: 10.2136/vzj2016.01.0010

Walvoord MA, Striegl RG. 2007. Increased groundwater to stream discharge from permafrost thawing in the Yukon River basin: Potential impacts on lateral export of carbon and nitrogen. *Geophysical Research Letters* **34** (12): L12402 DOI: 10.1029/2007GL030216

Williams PJ, Smith MW. 1989. *The Frozen Earth*. Cambridge University Press. DOI: 10.1017/CBO9780511564437

Woo M. 2012. *Permafrost Hydrology*. Heidelberg, Germany. DOI: 10.1657/1938-4246-45.4.615

Woo MK, Douglas LK, Carey SK, Yang D. 2008. Progress in Permafrost Hydrology in the New Millennium. *Permafrost and Periglacial Processes* **19**: 237–254 DOI: 10.1002/ppp

Wright N, Quinton WL, Hayashi M. 2008. Hillslope runoff from an ice-cored peat plateau in a discontinuous permafrost basin, Northwest Territories, Canada. *Hydrological Processes* **22** (15): 2816–2828 DOI: 10.1002/hyp.7005

Yukon Observational Well Network. 2001. Wolf Creek well. *Environment Yukon - Water Resources Branch*.

Zhang T. 2005. Influence of seasonal snow cover on the ground thermal regime: an overview. *Reviews in Geophysics* **43** (2004): RG4002 DOI: 10.1029/2004RG000157.1.INTRODUCTION

Zhang T, Osterkamp TE, Stamnes K. 1997. Effects of Climate on the Active Layer and Permafrost on the North Slope of Alaska, U.S.A. *Permafrost and Periglacial Processes* **8** (1): 45–67 DOI: 10.1002/(SICI)1099-1530(199701)8:1<45::AID-PPP240>3.0.CO;2-K

Zipper SC, Lamontagne-Hallé P, McKenzie JM, Rocha A V. 2018. Groundwater Controls on Postfire Permafrost Thaw: Water and Energy Balance Effects. *Journal of Geophysical Research: Earth Surface* (1): 2677–2694 DOI: 10.1029/2018JF004611

9 Supplementary Materials 1

9.1 North Facing Slope Well Log

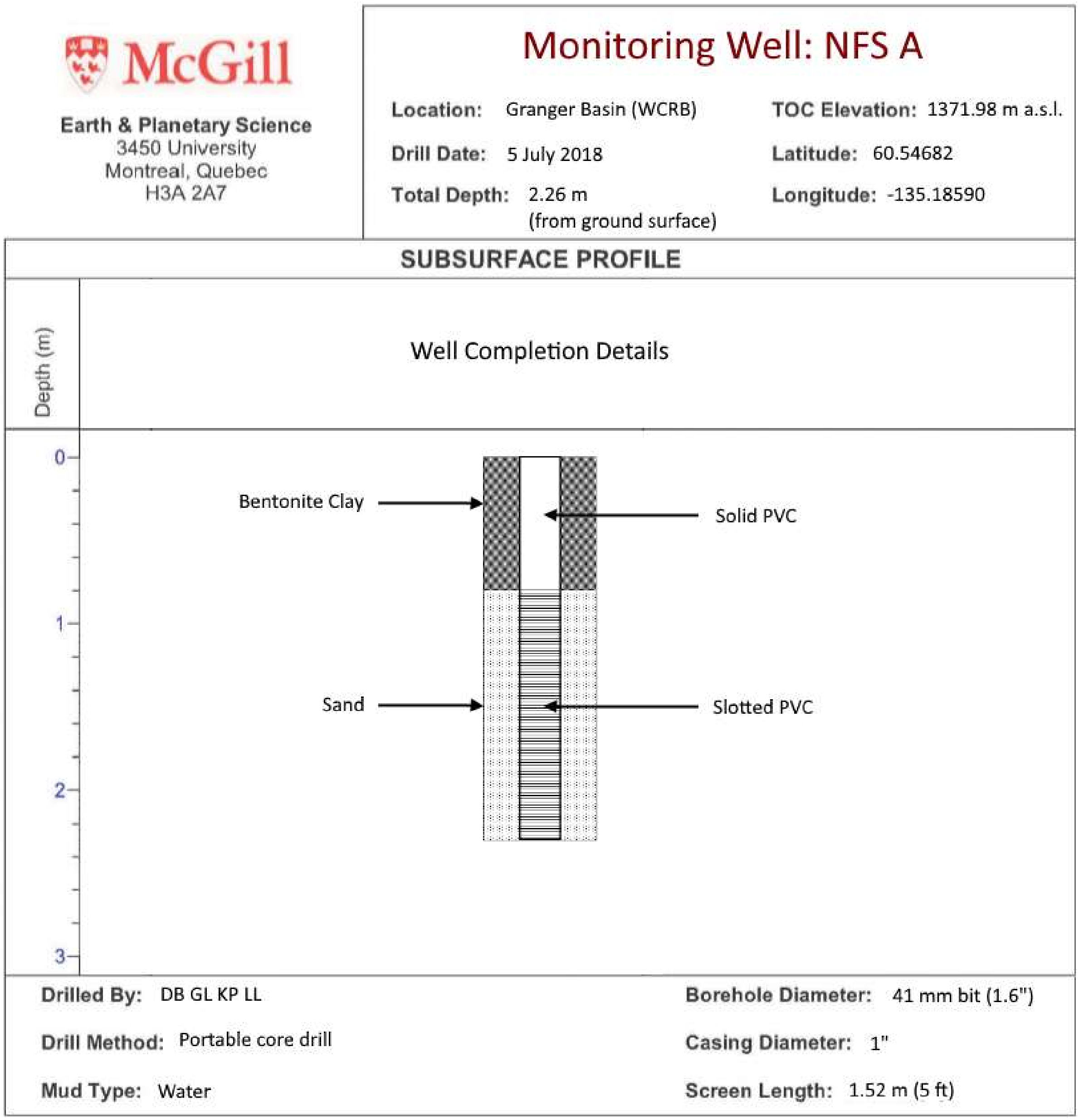

9.2 South Facing Slope Well Log

McGill

Earth & Planetary Science
3450 University
Montreal, Quebec
H3A 2A7

Monitoring Well: SFS A

Location: Granger Basin (WCRB)

Drill Date: 9 July 2018

Total Depth: 1.00 m (from ground surface)

TOC Elevation: 1373.28 m a.s.l.

Latitude: 60.54716

Longitude: -135.18588

SUBSURFACE PROFILE

Depth (m)

Well Completion Details

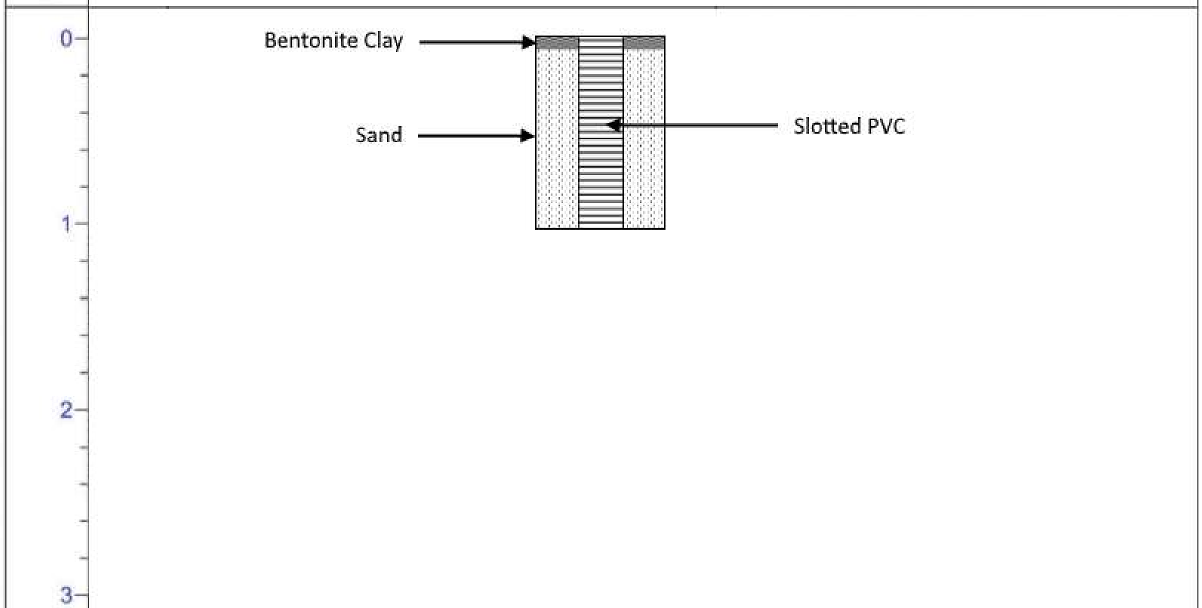

Drilled By: DB GL

Drill Method: Portable core drill

Mud Type: Water

Borehole Diameter: 51 mm bit (2.0")

Casing Diameter: 1"

Screen Length: 1.0 m

10 Supplementary Materials 2

The USGS Saturated-Unsaturated Transport Model (SUTRA) is a finite element numerical model that simulates groundwater flow and heat transfer (Voss and Provost, 2002). McKenzie *et al.* (2007) modified the code to include dynamic freeze-thaw functionality in variably saturated conditions, impacting variable permeability as function of ice content and the release or absorption of energy due to the latent heat of fusion. Further improvements were made by McKenzie and Voss (2013) to improve freeze-thaw processes and improve the impacts on fluid density. We use the unsaturated zone freeze-thaw processes presented in Briggs *et al.* (2014), and the version of SUTRA with improved boundary conditions described in Lamontage-Hallé *et al.* (2018).

10.1 SUTRA Governing Equations

The governing equation for groundwater flow used in this version of SUTRA is:

$$Q_P = \left[S_L P_L S_{op} + \varepsilon\left(\rho_L \frac{\partial S_L}{\partial p}\right)\right]\frac{\partial p}{\partial t} + \varepsilon\left(S_L \frac{\partial \rho_L}{\partial T}\right)\frac{\partial T}{\partial t} - \underline{\nabla} \cdot \left[\left(\frac{\underline{\underline{k}} k_r \rho_L}{\mu}\right)\left(\underline{\nabla} p - \rho_L g\right)\right] \qquad [1]$$

where S_{op} is specific pressure storativity ($L \cdot t^2 \cdot M^{-1}$), ε is the soil porosity, p is the pore water pressure ($M \cdot L^{-1} \cdot t^{-2}$), t is time, T is temperature, $\underline{\underline{k}}$ is the solid matrix permeability tensor (L^2), k_r is the relative permeability, μ is the fluid viscosity ($M \cdot L^{-1} \cdot S^{-1}$), g is the gravitational acceleration ($L \cdot t^{-2}$), Q_p is a fluid mass source ($M \cdot L^{-3} \cdot t^{-1}$), ρ_L is liquid water density ($M \cdot L^{-3}$) and S_L is the liquid water saturation.

The governing equation for energy transport is:

$$C_{eff}\frac{\partial T}{\partial t} = -\varepsilon S_L \rho_L c_L \underline{v} \cdot \left(\underline{\underline{\lambda_{eff}}} \underline{\nabla} T\right) + Q_P c_L (T^* - T) + \varepsilon S_L \rho_L \gamma_L + (1-\varepsilon)\rho_S \gamma_S \qquad [2]$$

where C_{eff} is the effective volumetric heat capacity of the matrix ($E \cdot L^{-3} \cdot {}^{\circ}C\text{-}^{1}$), c_L is the specific heat of liquid water ($E \cdot M^{-1} \cdot {}^{\circ}C^{-1}$), v is the average groundwater velocity vector ($L \cdot t^{-1}$), $\underline{\underline{\lambda_{eff}}}$ is the effective thermal conductivity tensor of the matrix ($E \cdot t^{-1} \cdot L^{-1} \cdot {}^{\circ}C^{-1}$), T^* is the temperature of the fluid, ρ_S is the solid grains density ($M \cdot L^{-3}$), and γ_L and γ_S are the energy sources in the water and solid grains, respectively ($E \cdot M^{-1} \cdot t^{-1}$).

The effective heat capacity (C_{eff}) is calculated using the weighted arithmetic average of the heat capacities of the matrix constituents including liquid water, ice, and solid grains. This includes the release or absorption of energy due to latent heat during water phase changes:

$$C_{eff} = \varepsilon(S_L \rho_L c_L + S_I \rho_I c_I) + (1-\varepsilon)\rho_S c_S - \Delta H_f \varepsilon \rho_I \frac{\partial S_I}{\partial T} \qquad [3]$$

where ΔH_f is the latent heat of fusion ($E \cdot M^{-1}$), S_I is the ice saturation, ρ_I is the ice density ($M \cdot L^{-3}$), and c_L, c_I , and c_S are the specific heats of liquid water, ice, and the solid grains, respectively ($E \cdot M^{-1} \cdot {}^{\circ}C^{-1}$).

The effective thermal conductivity of the matrix ($\underline{\underline{\lambda_{eff}}}$) is equal to the weighted average thermal conductivity of the matrix constituents including the thermal effects of mechanical dispersion:

$$\underline{\underline{\lambda_{eff}}} = [\varepsilon(S_L\lambda_L + S_I\lambda_I) + (1-\varepsilon)\lambda_S]\underline{\underline{I}} + \varepsilon S_L \rho_L c_L \underline{\underline{D}} \qquad [4]$$

10.2 Saturation and Permeability Functions

At each timestep, SUTRA calculates pressure and temperature for each node through the governing energy and water flow equations. For simulations with variable saturation, it employs a user-defined function to calculate total water saturation (S_w) based on the simulated pore pressure, ρ ($M \cdot L^{-1} \cdot t^{-2}$). Our study uses a user-defined piecewise-linear function (Lamontagne-Hallé *et al.*, 2018):

$$S_w = \begin{cases} 1 & \text{if } p > p_{ent} \\ (1-S_{wres})\left(\dfrac{p-p_{ent}}{p_{wres}-p_{ent}}\right) & \text{if } p_{ent} \geq p \geq p_{wres} \\ S_{wres} & \text{if } p < p_{wres} \end{cases} \qquad [5]$$

where p_{ent} is the air-entry value ($M \cdot L^{-1} \cdot t^{-2}$), S_{wres} is the residual liquid saturation, and p_{wres} is the suction at residual liquid saturation ($M \cdot L^{-1} \cdot t^{-2}$).

Liquid water saturation (S_L) varies exponentially with temperature, T (°C) and is calculated as (Mottaghy and Rath, 2006; Kozlowski, 2007; Kurylyk and Watanabe, 2013):

$$S_L = \begin{cases} 1 & if\ T \geq T_f \\ (1-S_{wres})e^{-\left(\frac{T-T_f}{W}\right)^2} + S_{wres} & if\ T < T_f \end{cases} \qquad [6]$$

if $S_L < S_W$ in unsaturated conditions, else $S_L = S_W$. T_f is the freezing temperature (°C) and W is the saturation model fitting parameter.

Permeability, k (L^2), of ground that is frozen, unsaturated, or both decreases with an impedance function (Hansson et al., 2004; Kurylyk and Watanabe, 2013; Evans and Ge, 2017):

$$k = k_{sat}10^{-\Omega(1-S_L)} \qquad [7]$$

where k_{sat} is the permeability of the unfrozen saturated permeability of the ground (L^2) and Ω is the impedance factor.

10.3 References

Briggs MA, Walvoord MA, McKenzie JM, Voss CI, Day-Lewis FD, Lane JW. 2014. New permafrost is forming around shrinking Arctic lakes, but will it last? *Geophysical Research Letters* DOI: 10.1002/2014GL059251

Evans, SG, Ge, S. 2017. Contrasting hydrogeologic responses to warming in permafrost and seasonally frozen ground hillslopes. *Geophys. Res. Lett*. 44, 2016GL072009. doi:10.1002/2016GL072009

Hansson, K, Šimůnek, J, Mizoguchi, M, Lundin, L-C, van Genuchten, MT. 2004. Water Flow and Heat Transport in Frozen Soil: Numerical Solution and Freeze–Thaw Applications. *Vadose Zone Journal*, 3, 693–704. doi:10.2113/3.2.693

Kozlowski, T. 2007. A semi-empirical model for phase composition of water in clay– water systems. *Cold Regions Science and Technology* 49, 226–236. doi:10.1016/j.coldregions.2007.03.013

Kurylyk, BL, Watanabe, K. 2013. The mathematical representation of freezing and thawing processes in variably-saturated, non-deformable soils. *Advances in Water Resources* 60, 160–177. doi:10.1016/j.advwatres.2013.07.016

McKenzie JM, Voss CI, Siegel DI. 2007. Groundwater flow with energy transport and water-ice phase change: Numerical simulations, benchmarks, and application to freezing in peat bogs. *Advances in Water Resources* DOI: 10.1016/j.advwatres.2006.08.008

McKenzie JM, Voss CI. 2013. Permafrost thaw in a nested groundwater-flow system. *Hydrogeology Journal* **21**: 299–316 DOI: 10.1007/s10040-012-0942-3

Mottaghy D, Rath V. 2006. Latent heat effects in subsurface heat transport modelling and their impact on palaeotemperature reconstructions. *Geophys. J. Int.* **164** 236–45

Lamontagne-Hallé P, McKenzie JM, Kurylyk BL, Zipper SC. 2018. Changing groundwater discharge dynamics in permafrost regions. *Environmental Research Letters*

Voss CI, Provost A. 2002. SUTRA: A model for 2D or 3D saturated-unsaturated, variable-density ground-water flow with solute or energy transport DOI: 10.3133/wri024231